



Review

Potential Novel Role of Membrane-Associated Carbonic Anhydrases in the Kidney

Seong-Ki Lee ^{1,*} , Walter F. Boron ^{1,2,3} and Rossana Occhipinti ^{1,*}

¹ Department of Physiology and Biophysics, School of Medicine, Case Western Reserve University, Cleveland, OH 44106, USA

² Department of Medicine, School of Medicine, Case Western Reserve University, Cleveland, OH 44106, USA

³ Department of Biochemistry, School of Medicine, Case Western Reserve University, Cleveland, OH 44106, USA

* Correspondence: seong-ki.lee@case.edu (S.-K.L.); rossana.occhipinti@case.edu (R.O.); Tel.: +1-216-368-5906 (S.-K.L.); +1-216-368-3631 (R.O.)

Abstract: Carbonic anhydrases (CAs), because they catalyze the interconversion of carbon dioxide (CO₂) and water into bicarbonate (HCO₃[−]) and protons (H⁺), thereby influencing pH, are near the core of virtually all physiological processes in the body. In the kidneys, soluble and membrane-associated CAs and their synergy with acid–base transporters play important roles in urinary acid secretion, the largest component of which is the reabsorption of HCO₃[−] in specific nephron segments. Among these transporters are the Na⁺-coupled HCO₃[−] transporters (NCBTs) and the Cl[−]-HCO₃[−] exchangers (AEs)—members of the “solute-linked carrier” 4 (SLC4) family. All of these transporters have traditionally been regarded as “HCO₃[−]” transporters. However, recently our group has demonstrated that two of the NCBTs carry CO₃^{2−} rather than HCO₃[−] and has hypothesized that all NCBTs follow suit. In this review, we examine current knowledge on the role of CAs and “HCO₃[−]” transporters of the SLC4 family in renal acid–base physiology and discuss how our recent findings impact renal acid secretion, including HCO₃[−] reabsorption. Traditionally, investigators have associated CAs with producing or consuming solutes (CO₂, HCO₃[−], and H⁺) and thus ensuring their efficient transport across cell membranes. In the case of CO₃^{2−} transport by NCBTs, however, we hypothesize that the role of membrane-associated CAs is not the appreciable production or consumption of substrates but the minimization of pH changes in nanodomains near the membrane.

Keywords: transporters; carbonate; bicarbonate; acid–base homeostasis; cell membranes; renal tubules



Citation: Lee, S.-K.; Boron, W.F.; Occhipinti, R. Potential Novel Role of Membrane-Associated Carbonic Anhydrases in the Kidney. *Int. J. Mol. Sci.* **2023**, *24*, 4251. <https://doi.org/10.3390/ijms24044251>

Academic Editor: Claudiu T. Supuran

Received: 24 January 2023

Revised: 6 February 2023

Accepted: 6 February 2023

Published: 20 February 2023



Copyright: © 2023 by the authors. Licensee MDPI, Basel, Switzerland. This article is an open access article distributed under the terms and conditions of the Creative Commons Attribution (CC BY) license (<https://creativecommons.org/licenses/by/4.0/>).

1. Introduction

Carbonic anhydrases (CAs) are ubiquitous metalloenzymes that play a fundamental role in numerous vital processes, including cellular metabolism, carbon dioxide (CO₂) and ion transport, and acid–base homeostasis [1–5]. These enzymes are important because they permit rapid interconversion of CO₂ and bicarbonate (HCO₃[−]), thereby promoting the rapid buffering of acid or alkali loads and facilitating—to various degrees—the diffusion of CO₂, HCO₃[−], H⁺, and other buffers [5]. For example, in red blood cells (RBCs), intracellular CA provides a mechanism for the efficient carriage of CO₂ from peripheral tissues to the lungs [5]. In the kidneys, as we shall see later, the synergistic action of soluble and membrane-associated CA activity permits efficient reabsorption of filtered HCO₃[−].

CAs are also linked to a variety of pathological processes, including renal tubular acidosis, osteopetrosis, osteoporosis, and tumor proliferation [6–12]. Inhibition of CAs has important pharmacological implications, for example, in the treatment of glaucoma, epilepsy, acute mountain sickness, and, more recently, even cancer [13–17]. CAs may also be useful as markers for cancer diagnosis [17–19].

Because of their involvement in physiological and pathological processes, these enzymes continue to be the focus of current investigations. CA was discovered in 1933 in

bovine RBCs by Meldrum and Roughton during their study of the interactions between CO_2 and HCO_3^- in blood [20]. The first three isozymes to be identified were CA A (later renamed CA III), CA B (later CA I), and CA C (later CA II) [21–24]. We now recognize eight evolutionally unrelated families of CAs: α -, β -, γ -, δ -, ζ -, η -, θ -, and ι -CAs [2,13,25–27]. α -CAs, which include CAs I–III, are found in numerous eukaryotic and prokaryotic organisms and are the most widely studied and characterized because of their importance in higher animals [28,29]. β -CAs are found in both eukaryotes (e.g., algae, plant chloroplast, and fungi) and prokaryotes. Recently, β -CAs have also been identified in animals, particularly in invertebrates [28–31]. γ -CAs are mainly found in archaea and some bacteria, and δ - and ζ -CAs are expressed in some marine diatoms [28,29,32]. The η -CAs are found in the protozoan *Plasmodium* species, which cause malaria in humans [33]. In the past few years, investigators have identified θ - [34] and ι -CAs [25] in marine diatoms.

While most CAs have a zinc ion (Zn^{2+}) in their active site, the γ - and ζ - families may contain different metals ions (e.g., iron [35] or cobalt [36] in γ -CAs and cadmium [37] in ζ -CAs). Some ι -CAs may not require any metal ion in their active site [27,38].

In this review, we focus exclusively on the α -family, which predominates among animals. The α -CA family comprises thirteen enzymatically active isozymes and three inactive ones. Figure 1 shows their different sub-cellular localizations (i.e., cytosolic, mitochondrial, secretory, and membrane-associated). Each member of the α -CA family has a distinct combination of kinetic properties and tissue-specific distribution. For example, CA II and CA III are both found in the cytosol but have the highest and lowest catalytic activities, respectively [39–41]. CA II is widely expressed throughout the body, whereas CA III is expressed mainly in muscle cells [2]. Moreover, members of the α -CA family have different susceptibilities to inhibitors. For example, CA II can be easily blocked by acetazolamide (ACZ) and topiramate (i.e., very small amounts of inhibitor can block enzyme activity). CA IV can be blocked more easily by ACZ than topiramate [42].

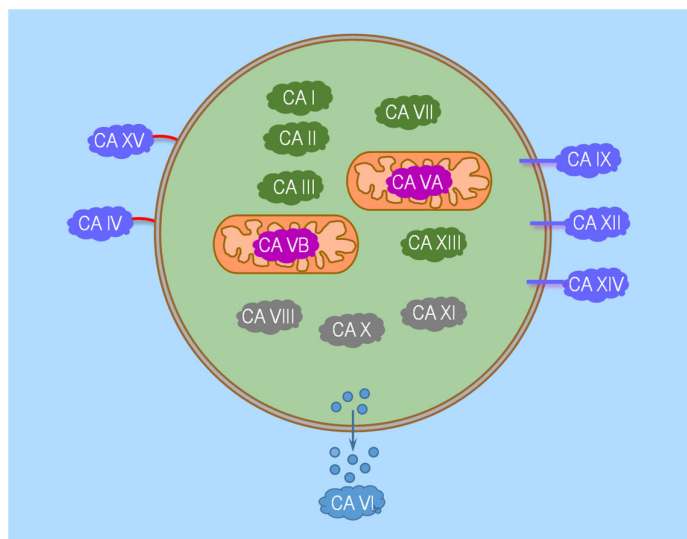


Figure 1. Cartoon illustrating the sub-cellular localization of the currently known α -CA family members. According to their sub-cellular localization, α -CAs can be classified into four groups: cytosolic (CA I, CA II, CA III, CA VII, CA VIII, CA X, CA XI, and CA XIII), mitochondrial (CA VA and CA VB), secretory (CA VI), and membrane-associated (CA IV, CA IX, CA XII, CA XIV, and CA XV). The cytosolic isozymes are all active (indicated in dark green) except for CA VIII, X, and XI (in grey), which are also called CA-related proteins (CARPs). Of the membrane-associated CAs, CA IV and CA XV are glycosylphosphatidylinositol (GPI)-linked, whereas CA IX, CA XII, and CA XIV are transmembrane. Note that the mitochondrial CA VA and CA VB are encoded by two different genes [43,44].

In the following sections, we examine the role of CA isozymes in renal acid–base physiology by reviewing established knowledge as well as new insights obtained by recent work from our group on the substrate identity of “HCO₃[−]” transporters of the “solute-linked carrier 4” (SLC4) family. After a brief overview of the members of the SLC4 family that play a role in renal acid–base physiology, we systematically review CA expression, sub-cellular localization, and functional interaction with SLC4 family proteins along the nephron segments that engage in acid secretion, including HCO₃[−] reabsorption. We conclude by suggesting that a role of membrane-associated CAs may be to reduce local pH changes caused by the transmembrane movement of carbonate (CO₃^{2−}) via the Na⁺-coupled HCO₃[−] transporter (NCBT) subfamily of SLC4 rather than to produce the substrate(s) for acid–base transport by NCBTs, as traditionally thought.

2. Catalytic Mechanism of α -Carbonic Anhydrases

In the absence of CAs, the interconversion of CO₂ and HCO₃[−] is a two-step bidirectional process:



In the first of the two sequential reactions (each governed by its own pK), CO₂ hydration describes the combination of CO₂ with water (H₂O) to form carbonic acid (H₂CO₃). Dehydration describes the opposite direction. In the second reaction, H₂CO₃ dissociates into HCO₃[−] and H⁺; this reaction, too, is reversible.

The two-step interconversion of CO₂ and HCO₃[−] is extremely slow because of the high activation energy of the first of the two reactions. A CA enzyme (activator) lowers the overall activation energy by bypassing the H₂CO₃ intermediate as the CA catalyzes the thermodynamically equivalent reaction:

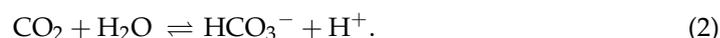


Figure 2 shows the catalytic mechanism of reaction (2) for all α -CAs. Known as the zinc-hydroxide mechanism [45,46], the central catalytic step—when viewed in the forward direction in reaction (2)—is the reaction of CO₂ with a zinc-hydroxide (i.e., Zn²⁺-OH[−]). The presence of the hydroxyl group rather than H₂O (i.e., Zn²⁺-H₂O, a less strong nucleophile than Zn²⁺-OH[−]) is necessary for the enzyme to be active and able to start the forward cycle [47].

In the state illustrated in the upper left of Figure 2, the Zn²⁺ of the α -CAs coordinates with three conserved histidine (His) residues and one hydroxyl group. Because in biological enzymes, Zn²⁺ can have up to six coordination sites, when α -CAs are in the Zn²⁺-OH[−] state, the Zn²⁺ has two free coordination sites [48,49]. In step #1 of the forward reaction cycle, the nucleophile O[−] (red-colored) in the hydroxyl group performs a nucleophilic attack on the carbon of CO₂ (green-colored), generating HCO₃[−] on the active site. An electron-rich O[−] (green-colored) on the HCO₃[−] molecule makes a fifth coordination with Zn²⁺. In step #2, H₂O interacts with Zn²⁺ via its O atom (blue-colored). This sixth coordination to Zn²⁺ destabilizes the two bonds between Zn²⁺ and HCO₃[−] so that, in step #3, HCO₃[−] dissociates from the enzyme active site. In step #4, Zn²⁺ acts as a Lewis acid, promoting deprotonation of the coordinated H₂O, thereby releasing H⁺ (blue-colored) and regenerating the Zn²⁺-OH[−] (we now morph the color from blue to red to restart the cycle) form of the enzyme [50].

The presence of different amino acids—with different positions and orientations—near the active site provides different catalytic activity and kinetics to the various CA isozymes. For example, the presence of histidine at position 64 (His-64) of CA II favors H₂O deprotonation (i.e., step #4 in Figure 2) by transferring H⁺ to the buffer in the media. Indeed, site-directed mutagenesis studies have shown that replacing this “shuttle histidine” with either alanine or glutamine inhibits CA II catalytic activity [51,52]. In the case of CA III—which has a structure very similar to that of CA II but much lower catalytic activity—substitution of the naturally occurring lysine-64 (in CA III) with His-64 enhances its enzymatic activity [39]. In addition, the presence of bulky amino acids next to His-64 in CA II, or

equivalently next to His-88 in CA IV, can also decrease catalytic activity. Other residues can modulate catalytic activity. Among them, threonine (Thr) 199 in CA II is important for stabilizing HCO_3^- in the active site by forming a network of hydrogen bonds [53,54].

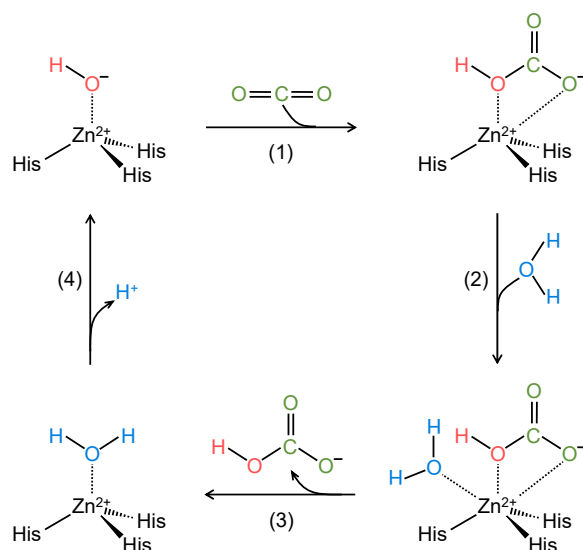


Figure 2. Schematics of the catalytic mechanism of action of α -CAs. In step #1, CO_2 (green-colored) reacts with a zinc-bound hydroxyl (OH^- , red-colored), generating a coordinated HCO_3^- . In step #2, H_2O (blue-colored) binds to zinc (Zn^{2+}). In step #3, HCO_3^- dissociates from Zn^{2+} , thereby leading to the catalytically inactive form of the enzyme. In step #4, release of a H^+ ion from the Zn^{2+} -bound H_2O molecule regenerates the Zn^{2+} -bound OH^- group, thereby restoring the catalytic active form of the enzyme. His = histidine residue.

The α -CA family members are all enzymatically active except for the three cytosolic forms CA VIII, X, and XI that, for lack of one or more of the three conserved histidine residues in the active site, are unable to perform the cycle illustrated in Figure 2. These three CAs are known as CA-related proteins (CARPs). Despite being apparently linked to various diseases, their physiological role is not well understood [55]. An intriguing possibility is that, like the CA-like domain of the receptor protein tyrosine phosphatase γ (see below), the CARPs may be molecular sensors of CO_2 and/or HCO_3^- .

3. Carbonic Anhydrases in Nanodomains Adjacent to the Cell Membrane

In addition to reactions (1) and (2) above, the chemistry of HCO_3^- also includes the dissociation of this species into carbonate (CO_3^{2-}) and H^+ :



In contrast to reaction (2), reaction (3) is very fast and does not rely on the action of a catalyst. Another difference is their respective pK values, ~ 6.1 at 37°C for reaction (2) and ~ 10.3 for reaction (3). As a consequence, reaction (2) is dominant at physiological pH , and the majority of CO_2 -related carbon species in the body is in the form of HCO_3^- .

It is informative to examine how the transmembrane movements of CO_2 , HCO_3^- , H^+ , and CO_3^{2-} as well as how membrane-associated CAs (all of which are on the outer surface of the plasma membrane; see Figure 1) affect the chemical equilibria of reactions (2) and (3).

When CO_2 , HCO_3^- , H^+ , or CO_3^{2-} move across a cell membrane, they perturb the chemical equilibria of reactions (2) and (3) in the nanodomain near the outer surface (oS) of the membrane, as illustrated in Figure 3. Comparable, though opposite, reactions occur at the inner surface of the membrane (not shown). In panels A–D, we orient all fluxes in the direction that would produce a fall in pH_{oS} . If CO_2 moves out of the cell (Figure 3A), CA tends to reestablish the chemical equilibrium of reaction (2) near the outer surface by consuming the exiting CO_2 (i.e., minimizing the rise in $[\text{CO}_2]_{\text{oS}}$) to produce HCO_3^- and

H^+ (i.e., accentuating the rise in $[H^+]_{oS}$ /fall in pH_{oS}). If CO_2 were entering the cell, the CA would do just the opposite. Thus, in both situations (i.e., independently of the direction of CO_2 movement), CA tends to minimize changes in $[CO_2]_{oS}$ but maximize changes in pH_{oS} .

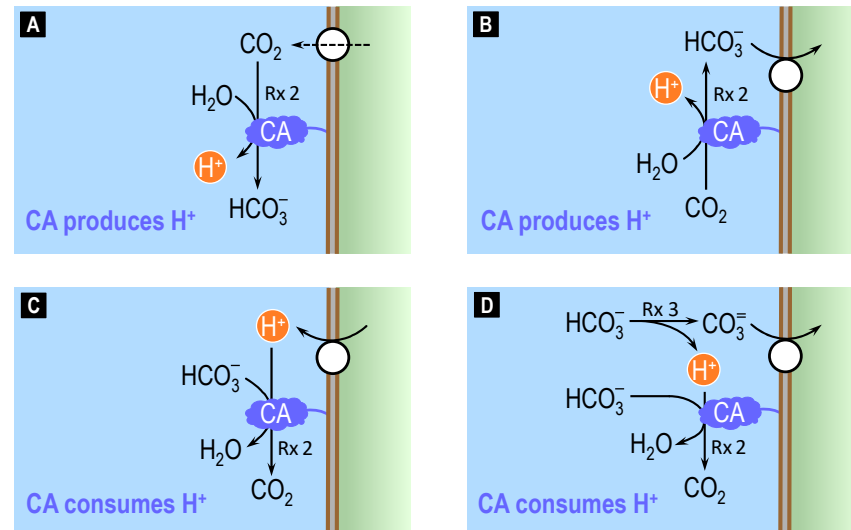


Figure 3. Interaction of fluxes of CO_2 , HCO_3^- , H^+ , and CO_3^{2-} with CA-catalyzed reactions on the outer surface of a cell. (A) If CO_2 exits the cell, CA tends to minimize the rise in $[CO_2]_{oS}$ at the outer surface (oS) of the cell membrane, and maximize the fall in pH_{oS} . (B) If HCO_3^- enters the cell, CA tends to minimize the fall in $[HCO_3^-]_{oS}$ and maximize the fall in pH_{oS} . (C) If H^+ exits the cell, CA tends to minimize the rise in $[H^+]_{oS}$ (i.e., minimize the fall in pH_{oS}). (D) If CO_3^{2-} enters the cell, CA tends to minimize the fall in $[CO_3^{2-}]_{oS}$ (indirectly) and the fall in pH_{oS} (directly). Rx = reaction; the number following the abbreviation 'Rx' indicates the numbering of the reaction in the main text. CA = carbonic anhydrase.

If HCO_3^- moves into the cell (Figure 3B), CA tends to produce HCO_3^- (i.e., minimizing the fall in $[HCO_3^-]_{oS}$) as well as H^+ (i.e., accentuating the rise in $[H^+]_{oS}$ /fall in pH_{oS}). If HCO_3^- were exiting the cell, the CA would do just the opposite. Thus, independently of the direction of HCO_3^- movement, the CA tends to minimize changes in $[HCO_3^-]_{oS}$ but maximize changes in pH_{oS} .

If H^+ moves out of the cell (Figure 3C), CA tends to consume H^+ (i.e., minimizing the rise in $[H^+]_{oS}$) as well as HCO_3^- (i.e., accentuating the fall in $[HCO_3^-]_{oS}$). If H^+ were entering the cell, the CA would do just the opposite. Thus, independently of the direction of H^+ movement, the CA tends to minimize changes in pH_{oS} .

A more complex scenario occurs when CO_3^{2-} moves across the cell membrane because CO_3^{2-} movement first produces a major perturbation in the chemical equilibrium of reaction (3) near the outer surface of the membrane, followed by a large secondary effect on the equilibrium of reaction (2) because $[HCO_3^-]_{oS} \gg [CO_3^{2-}]_{oS}$ under physiological conditions. If CO_3^{2-} enters the cell (Figure 3D), reaction (3) tends to replenish the lost CO_3^{2-} , thereby producing H^+ near the outer surface of the membrane. Catalyzing reaction (2), CA will then consume much of the newly formed H^+ . If CO_3^{2-} were exiting the cell, the CA would do just the opposite. Thus, independently of the direction of CO_3^{2-} movement, the CA tends to minimize not only changes in $[CO_3^{2-}]_{oS}$ but also changes in pH_{oS} .

In summary, all four panels in Figure 3 show us that CA near the membrane tends to stabilize the concentration of the transported solute, regardless of direction. Based on intuition, one might predict that these actions, in principle, would universally accelerate transport. However, this is not true. In the case of CO_2 (Figure 3A), the work from our group [56–58]—which extends the earlier work of Gutknecht and colleagues [59]—shows that the stimulation of CO_2 transport by CAs is quite large. The reason is that the CA-catalyzed reaction can have very large effects on $[CO_2]_{oS}$ because $pH_{oS} \gg pK$, so that $[HCO_3^-]_{oS} \gg [CO_2]_{oS}$. In the case

of HCO_3^- (Figure 3B), CA has negligible effects on the transport rate, as described below. We would expect as much: because $[\text{HCO}_3^-]_{\text{OS}} \gg [\text{CO}_2]_{\text{OS}}$ under physiological conditions, the CA-catalyzed reaction has little impact on $[\text{HCO}_3^-]_{\text{OS}}$. In the case of H^+ (Figure 3C), the effect of CA on transport rate has, to our knowledge, not been tested. However, we suspect that the impact of CA might be muted, again because the high $[\text{HCO}_3^-]_{\text{OS}}/[\text{CO}_2]_{\text{OS}}$ ratio would tend to reduce the extent of the forward reaction in Figure 3C. Finally, in the case of CO_3^{2-} (Figure 3D), CA has a negligible impact on the transport rate, as we discuss below. We would expect as much: because $[\text{HCO}_3^-]_{\text{OS}} \gg \gg [\text{CO}_3^{2-}]_{\text{OS}}$ under physiological conditions, the rate of the reaction $\text{HCO}_3^- \rightarrow \text{CO}_3^{2-} + \text{H}^+$ is apparently little influenced by CA-dependent changes in $[\text{H}^+]_{\text{OS}}$.

Continuing the summary, the upper row of Figure 3 shows that, for fluxes of CO_2 (Figure 3A) or HCO_3^- (Figure 3B), CA magnifies pH changes in the nanodomain near the membrane. Conversely, the lower row of Figure 3 shows that, for fluxes of H^+ (Figure 3C) or CO_3^{2-} (Figure 3D), CA minimizes pH changes in the nanodomain near the membrane.

Below, we show that it is possible to exploit the chemistry of reactions (2) and (3), as well as a variety of biophysical approaches, to identify the substrates carried by “ HCO_3^- ” transporters.

4. Carbonic Anhydrases and the Identification of Substrates of SLC4 Family Members

In theory, “ HCO_3^- ” transporters could carry any of the solutes involved in reactions (2) and (3). Distinguishing among them has been challenging because, in contrast with non-labile ions (e.g., sodium, potassium), the solutes of reactions (2) and (3) are interchangeable (i.e., they can be converted into each other), making direct measurements virtually impossible. Some investigators have resorted to surrogate substrates or kinetic approaches [60–66]. However, neither approaches are definitive: (i) No surrogate can mimic the real physicochemical properties of the substrates under consideration [67]. (ii) The only definitive conclusion that can come from kinetic approaches—and even then, only under favorable circumstances—is to rule out false hypotheses. Although kinetic studies can support a model, they can never rule one out. Thus, although various investigators may have had their hypotheses based on surrogate or kinetic data, none of these conclusions—by definition—could have been definitive.

An advancement towards solving this technical conundrum was the theoretical observation that the combination of CA inhibitors and their opposite effects on pH changes could help distinguish HCO_3^- vs. CO_3^{2-} transport across cell membranes [68–70]. However, early studies with CA inhibitors and pH measurements could not determine unambiguously the identity of the transported substrate because of limitations in the experimental system (native tissue), which almost certainly comprised an unknown mixture of acid–base transporters. Moreover, in these earlier studies, the investigators did not consider the possibility that “ HCO_3^- ” transporters could carry H^+ or CO_2 . Interestingly, preliminary work from our group suggests that the electrogenic Na/ HCO_3^- cotransporter-1 (variant A) can conduct CO_2 [71,72].

In the following sections, after a brief overview of the members of the SLC4 family of “ HCO_3^- ” transporters, we review a recent study from our group in which we were able to identify unambiguously the nature of the substrates carried by the “ HCO_3^- ” transporters of the SLC4 family.

4.1. Brief Overview of the SLC4 Family Members

Mammalian “ HCO_3^- ” transporters belong to two major gene families, namely SLC4 and SLC26. Nine of the ten SLC4 members carry “ HCO_3^- ”. To date, some members of the SLC26 family appear to carry “ HCO_3^- ” [73,74], an example of which is SLC26A4 or pendrin [75,76]. In addition, HCO_3^- can cross membranes via Cl^- channels, such as the cystic fibrosis transmembrane conductance regulator (CFTR) and γ -aminobutyric acid (GABA) receptor channel [77].

Here, we focus on the members of the SLC4 family that carry “HCO₃[−]” because of their predominant role in renal HCO₃[−] reabsorption.

The mammalian SLC4 family includes ten genes (*SLC4A1-5*; *SLC4A7-11*) that encode a group of ten functionally diverse integral membrane proteins. All but *SLC4A11* encode proteins that transport HCO₃[−] or a HCO₃[−]-related species, such as CO₃^{2−}—we refer to all of these substrates as “HCO₃[−]”. These transporters can be either Na⁺-independent or Na⁺-dependent. The three Na⁺-independent members are the anion exchangers (AE1-3; products of *SLC4A1-3* genes), which carry HCO₃[−] in exchange for Cl[−]. The five Na⁺-dependent members are the Na⁺-coupled bicarbonate transporters (NCBTs), which carry Na⁺ and “HCO₃[−]” in the same direction. The NCBTs include the two electrogenic Na⁺/HCO₃[−] cotransporters NBCe1 (*SLC4A4*) and NBCe2 (*SLC4A5*) that carry electrical current, the two electroneutral Na⁺/HCO₃[−] cotransporters NBCn1 (*SLC4A7*) and NBCn2 (*SLC4A10*), and the electroneutral Na⁺-driven Cl[−]/HCO₃[−] exchanger NDCBE (*SLC4A8*). The remaining ninth “HCO₃[−]” transporter is the protein encoded by *SLC4A9*, currently named AE4. However, despite being called AE4, it is still controversial whether this protein is a Na⁺-independent Cl[−]/HCO₃[−] exchanger [78–80] or a Na⁺-dependent HCO₃[−] transporter [81,82]. A tenth member of the SLC4 family is the bicarbonate transporter-related protein-1 (BTR1, *SLC4A11*), which is no longer believed to be a HCO₃[−] transporter but rather a H⁺ (or OH[−]) conducting protein [83,84].

Members of the SLC4 family are expressed throughout the body and are essential for regulating intracellular and whole-body pH, and for transporting acid–base equivalents across many epithelia. These proteins are implicated in a variety of diseases. For example, mutations of AE1 have been associated with type I distal renal tubular acidosis (RTA) and hereditary spherocytosis [85–87]. Mutations of NBCe1 have also been linked to type II proximal RTA, glaucoma, migraine, and suicidal ideation [88–90].

Many reviews on the SLC4 family are available, and we refer the interested reader to these for more details (refs. [91–93]).

4.2. Theoretical Role of Carbonic Anhydrase in Distinguishing Bicarbonate versus Carbonate versus Proton Transport across Cell Membranes

Figure 4 illustrates the three possible models of acid–base transport that we explored in our study [73]: HCO₃[−] influx (panel A), CO₃^{2−} influx (panel B), and CO₂/HCO₃[−]-stimulated H⁺ efflux (panel C). For simplicity, we consider only the case in which a base enters the cell. Similar conclusions can be reached for the case in which a base exits the cell. We also omit the accompanying movements of Na⁺ and/or Cl[−] and the corresponding postulated transporter stoichiometry of the members of the SLC4 that we studied.

If the transporter mediates HCO₃[−] entry into the cell (Figure 4A), the result will be a decrease in [HCO₃[−]]_{o5}. The lost HCO₃[−] can be replenished by either diffusion (indicated by the dashed arrow), which does not affect pH_{o5} or reaction (2). Because reaction (2) produces H⁺, it will cause a decrease in pH_{o5} (see inset, lower left corner of panel A: solid black trace). Blocking CA (i.e., applying a CA inhibitor) will reduce H⁺ production, thereby causing a smaller decrease in pH_{o5} (dashed red trace).

If the transporter mediates CO₃^{2−} entry into the cell (Figure 4B), the result will be a decrease in [CO₃^{2−}]_{o5} that triggers reaction (3), thereby replenishing CO₃^{2−} but also producing H⁺. The consequence is a decrease in pH_{o5} (inset: solid black trace). Consuming some of this newly formed H⁺ will be reaction (2) catalyzed by CA. Therefore, blocking CA will reduce H⁺ consumption via reaction (2), causing a further decrease in pH_{o5} (dashed red trace). Thus, the blockade of CA in model A vs. model B has opposite effects on pH_{o5}.

If the transporter, stimulated by CO₂ or HCO₃[−], mediates H⁺ efflux from the cell (Figure 4C), the result will be an immediate increase in [H⁺]_{o5}, as reflected by a fall in pH_{o5} (inset: solid black trace). This triggers both H⁺ diffusion away from the membrane and the CA-catalyzed reaction (2), both of which mitigate the rise in [H⁺]_{o5}. Blocking CA will slow H⁺ consumption, magnifying the decrease in pH_{o5} (dashed red trace).

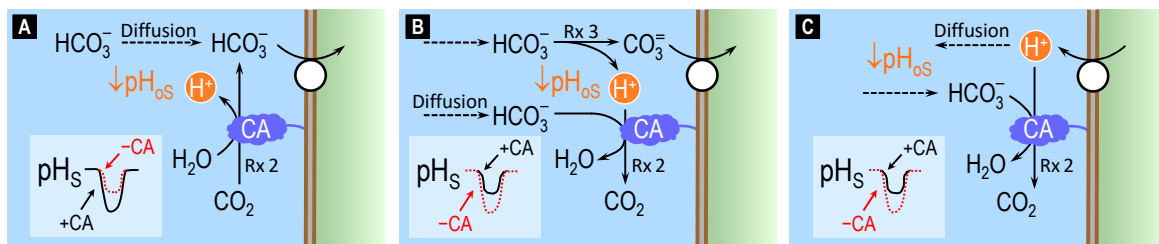


Figure 4. Theory of bicarbonate influx vs. carbonate influx vs. proton efflux across cell membranes. (A) The entry of HCO_3^- into the cell leads to the production of H^+ (i.e., a decrease in pH_{os} ; inset, lower left corner: solid black trace) via the CA-catalyzed reaction $\text{CO}_2 + \text{H}_2\text{O} \rightarrow \text{HCO}_3^- + \text{H}^+$ (indicated as 'Rx 2') at the outer surface (oS) of the cell membrane. Blocking CA (i.e., applying a CA inhibitor) reduces H^+ production (i.e., the decrease in pH_{os} ; dashed red trace). (B) The entry of CO_3^{2-} into the cell leads to the production of H^+ (i.e., a decrease in pH_{os} ; solid black trace) via the reaction $\text{HCO}_3^- \rightarrow \text{CO}_3^{2-} + \text{H}^+$ (indicated as 'Rx 3') at the outer surface of the cell membrane. Blocking CA (i.e., applying a CA inhibitor) reduces H^+ consumption by 'Rx 2' (i.e., increases the fall in pH_{os} ; dashed red trace). (C) The exit of H^+ from the cell leads to an immediate increase in $[\text{H}^+]_{\text{os}}$ (i.e., a decrease in pH_{os} ; solid black trace) which is mitigated by the CA-catalyzed reaction $\text{HCO}_3^- + \text{H}^+ \rightarrow \text{CO}_2 + \text{H}_2\text{O}$ at the outer surface of the cell membrane. Blocking CA (i.e., applying a CA inhibitor) reduces H^+ consumption by 'Rx 2' (i.e., increases the fall in pH_{os} ; dashed red trace). In model (C), the effect of blocking CA is the same as in model (B). Rx = reaction; the number following the abbreviation 'Rx' indicates the numbering of the reaction in the main text. CA = carbonic anhydrase.

Comparing the hypothetical solid black vs. the dashed red traces in the insets of Figure 4A–C, we see that the effect of CA blockade on the direction of the pH_{os} change should, in principle, allows one to distinguish HCO_3^- transport on the one hand (Figure 4A) from CO_3^{2-} or H^+ transport on the other (Figure 4B,C).

4.3. Surface pH Studies Supporting Carbonate as the Substrate of NCBTs

In order to test the three possible models of transport in Figure 4, we co-expressed in oocytes (i) NBCe1-A \pm CA IV as a test case for electrogenic NCBTs; (ii) AE1 \pm CA IV as a test case for electroneutral AEs and (iii) NDCBE \pm CA IV as an additional test case for electroneutral NCBTs. In all of these three cases, we exploited (i) the chemistry of reactions (2) and (3) at the outer surface of the plasma membrane, (ii) the CA inhibitor acetazolamide (ACZ), (iii) measurements of pH_{os} , (iv) heterologous expression of the proteins in *Xenopus* oocytes, and (v) mathematical simulations.

NBCe1-A appears to mediate the isodirectional movement of 1 Na^+ and 2 HCO_3^- ions (i.e., 1:2 stoichiometry), [93,94], as we could represent by doubling all stoichiometry values in Figure 4A. In principle, NBCe1-A could also move 1 Na^+ and 1 CO_3^{2-} in the same direction, as indicated by Figure 4B, or 1 Na^+ and 2 H^+ in the opposite direction in a CO_2 or HCO_3^- stimulated process, as we could represent by doubling all stoichiometry in Figure 4C. All three models are thermodynamically equivalent.

Because NBCe1-A is electrogenic, we simultaneously measured changes in NBC current (I_{NBC}) and pH_{os} with microelectrodes by shifting membrane voltage (V_m) using two-electrode voltage clamping technique. Details on this technical approach can be found in ref. [95]. Our data show that inhibition of CA IV by ACZ amplifies pH_{os} changes, thereby allowing us to rule out HCO_3^- transport (i.e., Figure 4A).

In order to distinguish between the transport of 1 Na^+ and 1 CO_3^{2-} in the same direction vs. 1 Na^+ and 2 H^+ in opposite directions, we introduced a powerful new set of tools: we analyzed the amount of H^+ that appears at the cell surface (measured as a change in pH_{os}) per electrical charge carried (e^- , measured as change in I_{NBC}) in each model. Using the well-characterized H^+ channel H_V1 to calibrate our experimental data and a reaction-diffusion mathematical model that simulates our experiments with oocytes, we were able to predict the amount of H^+ / e^- that appears at the cell surface. The

mathematical model is an extension of the one employed in previous studies [56–58] and includes reactions (1) and (3) as well as the non-CO₂/HCO₃[−] buffers (i.e., HEPES in the extracellular space to mimic the composition of our perfusion solution and the intrinsic cytosolic buffers). Comparing the model prediction with our experimental data, we were able to rule out both the Na⁺ + 2 HCO₃[−] model (simulation predicted very low H⁺/e[−]; see Figure 5A in Ref. [73]) and the Na⁺-2H⁺ exchange model (simulation predicted very high H⁺/e[−]; see Figure 5C in Ref. [73]). In fact, our data matched very closely the predictions for the transport of CO₃^{2−} (simulation predicted moderate H⁺/e[−]; see Figure 5B in Ref. [73]). Thus, we definitively conclude that NBCe1-A cannot carry either HCO₃[−] or H⁺ and most likely carries 1 Na⁺ and 1 CO₃^{2−} in the same direction.

In the cases of the electroneutral transporters AE1 and NDCBE, we could not use the H⁺/e[−] approach. Instead, we acid loaded the cytoplasm of oocytes by exposure to CO₂/HCO₃[−] (the CO₂ enters the cell and generates HCO₃[−] + H⁺) and then used intracellular-pH microelectrodes to monitor the subsequent recovery (i.e., increase) of intracellular pH (pH_i), which reflects the activity of the transporter. In addition, we monitored pH_{o5} changes during the rise in pH_i.

Our data on AE1 show that inhibition of CA IV by ACZ reduces pH_{o5} changes, thereby allowing us to rule out the transport of CO₃^{2−} (Figure 4B) or H⁺ (Figure 4C) and confirm what investigators had long believed; namely, AE1 transports HCO₃[−] (Figure 4A).

Our data on NDCBE show that inhibition of CA IV by ACZ amplifies pH_{o5} changes—the opposite of what we observed with AE1—thereby allowing us to rule out HCO₃[−] transport (Figure 4A).

In summary, our study shows that NBCe1-A almost certainly carries CO₃^{2−} or a related substrate (e.g., the NaCO₃[−] ion pair: NaHCO₃[−] ⇌ Na⁺ + CO₃^{2−}), AE1 does indeed carry HCO₃[−], and NDCBE does not carry HCO₃[−]. We suggest that similar studies will likely show that all AEs transport HCO₃[−] and all NCBTs transport CO₃^{2−}.

Finally, our approach can also be used for clarifying the nature of the substrates of transporters (e.g., SLC26 transporters) and channels that traditionally have been thought to mediate the movement of “HCO₃[−]”.

5. Relative Abundance of Members of the SLC4 and α-CA Families in Human Kidney

Before systematically examining the members of the SLC4 and α-CA families involved in renal HCO₃[−] reabsorption, we used data from a recently published human study to obtain information on the relative abundance of mRNA and proteins in the kidney [96]. Although the transcriptome analysis is comprehensive and unbiased, the protein expression is relative to the tissue with the highest expression of that protein. Therefore, we cannot truly compare relative amounts of different proteins in the kidney. In some cases, mRNA and protein levels do not correlate well. The study’s authors suggest that this discrepancy could be due to the specificity and affinity of different antibodies directed to different proteins, as well as the non-linearity of immunohistochemistry assays, or to post-translational modifications of proteins (e.g., secretion and proteolysis). We note that static mRNA levels do not need to correlate with static protein levels, let alone with the disposition of the protein (e.g., cellular localization, posttranslational modification) that is physiologically relevant. Thus, even though these data represent an impressive amount of work and may provide important insights for further experiments, one must interpret such data with caution.

The results of this study [96] are included in the Human Protein Atlas database (see “<http://www.proteinatlas.org/>”) (accessed on 20 January 2023).

5.1. SLC4 Family Members

Based on the RNAseq data of Fagerberg and coworkers [96], we classify the nine members of the SLC4 family that carry “HCO₃[−]” into four major categories (very low, low, medium, and high), using the normalized tags per million (nTPM) value as an index of mRNA level (Table 1). For proteins, we simply use Fagerberg’s categories (as low,

medium, and high) to describe expression levels [96]. It is noteworthy—but see caveats above regarding protein values—that *SLC4A4* (NBCe1) has both high mRNA and protein values. On the other hand, *SLC4A7* (NBCn1) and *SLC4A10* (NBCn2) both have very low or low mRNA levels but high protein values.

Table 1. Classification of human SLC4 family members that carry “HCO₃[−]” in the kidney. mRNA and protein expression levels were classified based on the study [96]. Very low: ≤5 nTPM; low: 5 ≤ 15 nTPM; medium: 15 ≤ 50 nTPM; high: >50 nTPM. * N/A means either not tested or not detected. nTPM = normalized tags per million.

Gene (Protein) Name	mRNA Expression				Protein Expression			
	Very Low	Low	Medium	High	Low	Medium	High	N/A *
<i>SLC4A1</i> (AE1)				x		x		
<i>SLC4A2</i> (AE2)			x			x		
<i>SLC4A3</i> (AE3)		x						x
<i>SLC4A4</i> (NBCe1)				x			x	
<i>SLC4A5</i> (NBCe2)	x					x		
<i>SLC4A7</i> (NBCn1)		x					x	
<i>SLC4A8</i> (NDCBE)	x							x
<i>SLC4A9</i> (AE4)			x					x
<i>SLC4A10</i> (NBCn2)	x						x	

Below, we provide information on current knowledge of cellular and sub-cellular localization of members of this family along the nephron.

5.2. α -CA Family Members

For the 15 human α -CA family members (note: humans lack *CA15*), Table 2 summarizes the mRNA and protein expression levels following the same approach that we employed for the SLC4 family. We note that the *CA2* and *CA12* genes produce both the highest nTPM and protein values. On the other hand, *CA4* has medium mRNA but low protein levels.

Table 2. Classification of human α -CA family members in the kidney. mRNA and protein expression levels were classified based on the study [96]. Very low: ≤1 nTPM; low: 1 ≤ 15 nTPM; medium: 15 ≤ 50 nTPM; high: >50 nTPM. * N/A means either not tested or not detected. nTPM = normalized tags per million. Note that no data are available for *CA15* because this gene has not been identified in humans [97].

Gene (Protein) Name	mRNA Expression				Protein Expression			
	Very Low	Low	Medium	High	Low	Medium	High	N/A *
<i>CA1</i> (CA I)		x						x
<i>CA2</i> (CA II)				x			x	
<i>CA3</i> (CA III)		x						x
<i>CA4</i> (CA IV)			x		x			
<i>CA5A</i> (CA VA)	x							x
<i>CA5B</i> (CA VB)		x				x		
<i>CA6</i> (CA VI)	x							x
<i>CA7</i> (CA VII)	x							x
<i>CA8</i> (CA VIII)		x						x
<i>CA9</i> (CA IX)	x							x
<i>CA10</i> (CA X)		x						x
<i>CA11</i> (CA XI)		x						x
<i>CA12</i> (CA XII)				x			x	
<i>CA13</i> (CA XIII)		x				x		
<i>CA14</i> (CA XIV)	x							x

These results are consistent with our current knowledge that CA II and CA XII are highly expressed in the kidneys but apparently are in conflict with the current impression that CA IV is similarly important. However, see the caveats above regarding reported protein levels. Note that CA IX overexpression has been associated with renal carcinoma [17].

Below, we provide information on current knowledge of cellular and sub-cellular localization of members of this family along the nephron.

6. Carbonic Anhydrases along the Nephron

The first report of CA activity in the kidneys dates back to 1941 when Davenport and Wilhelmi detected CA activity in the renal cortex of dogs, cats, and rats [98]. The identification of CA in the kidney was an important step toward understanding renal acid–base physiology.

The role of CA in urinary acidification emerged when investigators observed that the administration of CA inhibitors reduces the titratable acidity of the urine. Höber was the first to report that the addition of sulfanilamide in the perfusion fluid blocks urinary acidification in frog kidneys [99]. Studies by Pitts and Alexander also supported the role of CA in urinary acidification. These authors demonstrated that the two theories prevailing at the time on the mechanism of urinary acidification—reabsorption of bicarbonate vs. reabsorption of alkaline phosphate—could account only for a relatively small fraction of the maximum titratable acidity of the urine. Thus, they suggested that secretion of H^+ into the lumen was the only mechanism that could explain the amount of acid in the urine [100–104]. Pitts and Alexander correctly hypothesized that secretion of H^+ in renal tubules occurs in exchange for some filtered luminal cation, most likely Na^+ (as postulated earlier by Homer Smith [105,106]). Moreover, experiments with sulfonamide led these authors to suggest that the likely source of secreted H^+ was intracellular CO_2 hydration and that intracellular CA catalysis was an important part of this process [101]. During this time, the distal tubule was considered the main site of urinary acidification. Although some investigators had also suggested that the proximal tubule (PT) could play a role in urinary acidification [107–109], it was only in 1960 that Gottschalk and colleagues provided direct evidence on proximal acidification [110]. By performing microperfusion studies in rat kidneys, these authors observed that the fluid of the PT acidified to a pH of ~ 6.8 , consistent with the hypothesis that most bicarbonate reabsorption ($>85\%$) occurs in this segment.

Micropuncture and microperfusion studies exploiting CA inhibitors demonstrate that HCO_3^- reabsorption in PTs (i) strongly depends on the presence of luminal/membrane-associated and cytosolic CA and (ii) occurs via H^+ secretion into the lumen and not by direct absorption of HCO_3^- across the apical membrane [111–115]. Burg and colleagues, working with isolated perfused tubules, demonstrated that the PT and thick ascending limb (TAL) are major nephron segments responsible for reabsorbing HCO_3^- and that they both rely on CA and a Na-coupled H^+ -secretion mechanism [116–119]. McKinney and Burg confirmed that the collecting duct contributes to urinary acidification by reabsorption of bicarbonate in a CA-dependent manner [116]. However, contrary to what had been believed, they found that H^+ secretion in this segment is independent of Na^+ transport [116].

Our current knowledge of renal CA and its localization along the nephron is the result of numerous biochemical, immunocytochemical, and histochemical studies [24,120–126]. In 1975 Wistrand and coworkers, by employing affinity-chromatography techniques, were able to isolate CA from human kidneys and demonstrate that this CA was the same CA II of human RBCs [122]. These authors observed that a small percentage of the CA activity is not cytosolic but originates from a membrane-associated CA localized in both apical and basolateral membranes [127]. We now know that CA II, CA IV, and CA XII are the most prominent CA isozymes in the human kidney, with cytosolic CA II accounting for over 95% of the total renal CA activity and membrane-associated CA IV and CA XII accounting for the remaining 5% [24,111,120]. Although CA XIV is apparently not important in the human kidney, and the human genome lacks the *CA15* gene, both of these membrane-associated CAs play a role in the rodent kidney [2,120].

Below we describe the mechanisms of HCO_3^- reabsorption along the nephron with special emphasis on our current knowledge about the localization and functional role of the three renal CA isozymes in humans. The same proteins or processes that mediate HCO_3^- reabsorption also generate “new HCO_3^- ”. The only difference is that, in the case of HCO_3^- reabsorption, the H^+ secreted into the lumen titrates HCO_3^- , whereas in the case of new- HCO_3^- formation, the secreted H^+ titrates NH_3 (producing NH_4^+ secretion) or buffers like phosphate and creatinine (producing titratable acidity).

6.1. Proximal Tubule

PTs are responsible for reabsorbing ~80% to ~85% of filtered HCO_3^- . Most of this HCO_3^- (after the luminal reaction $\text{HCO}_3^- + \text{H}^+ \rightarrow \text{H}_2\text{O} + \text{CO}_2$) moves in the form of CO_2 from the lumen, across the apical membrane (AM), and into the cytosol. After reconversion to HCO_3^- , the carbon crosses the basolateral membrane (BLM) in the form of CO_3^{2-} or HCO_3^- .

Figure 5 illustrates the mechanisms of the preceding series of events. Mediating the majority of the H^+ secretion at the AM is Na-H exchanger 3 (NHE3), which uses the inward Na^+ gradient—established by the Na-K pump at the BLM—to exchange luminal Na^+ for intracellular H^+ [128–130]. Mediating a smaller fraction of H^+ secretion is the apical vacuolar-type H^+ pump (or V-type H^+ pump), which uses ATP hydrolysis to energize the extrusion of H^+ from the cell. A recent study on rat kidneys indicates that one variant of NBCn2 is present in the AM, where it could be responsible for the direct reabsorption of perhaps 20% of the reclaimed HCO_3^- [131].

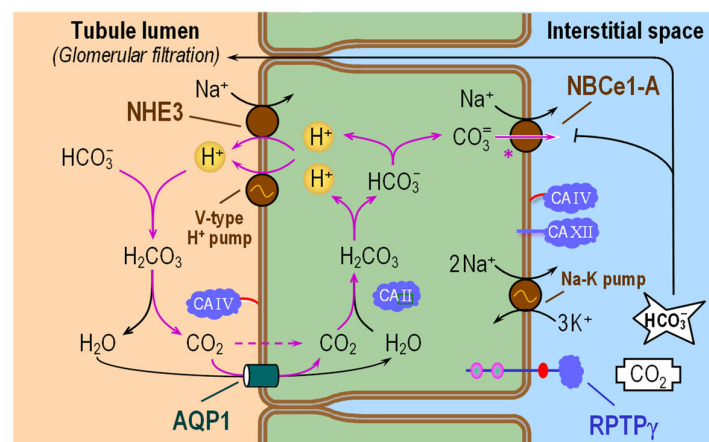


Figure 5. Cell model of HCO_3^- reabsorption in renal proximal tubule. In the lumen, filtered HCO_3^- and H^+ —secreted by NHE3 and V-type H^+ pump—react to form CO_2 and H_2O under the catalytic action of CA IV. Apical entry of CO_2 and H_2O via AQP1 leads to the intracellular formation of HCO_3^- and H^+ under the catalytic action of CA II. NBCe1-A carries CO_3^{2-} (further ionized form of HCO_3^-) out of the cell across the basolateral membrane. The pink symbol ‘*’ near NBCe1-A denotes uncertainty about NBCe1-A stoichiometry. For details, see text. NHE3 = Na-H exchanger 3; V-type H^+ pump = Vacuolar-type H^+ pump (or V-ATPase); AQP1 = aquaporin 1; CA II, CA IV and CA XII = carbonic anhydrase II, IV and XII; NBCe1-A = electrogenic Na/ HCO_3 cotransporter (1 variant A); RPTP γ = receptor protein tyrosine phosphatase- γ .

In the lumen, secreted H^+ combines with filtered HCO_3^- , thereby producing CO_2 and H_2O under the catalytic action of CA IV. The newly formed CO_2 and H_2O cross the AM mostly through the water channel aquaporin AQP1 [132–135]. In the cytosol, CA II promotes rapid conversion of CO_2 and H_2O into HCO_3^- and the first of two H^+ . This newly formed H^+ then recycles back into the lumen, whereas the newly produced HCO_3^- will further dissociate to form a second H^+ plus CO_3^{2-} and exit the cell across the BLM in the form of CO_3^{2-} via NBCe1-A [136]. This second H^+ also recycles back into the lumen. Because the debate continues as to whether, in PT cells, NBCe1-A truly operates

with a $1\text{Na}^+:3\text{HCO}_3^-$ stoichiometry or, as in most other cells, with a $1\text{Na}^+:2\text{HCO}_3^-$ stoichiometry, in Figure 5 we show a single CO_3^{2-} only (i.e., consistent with a 1:2 stoichiometry). An apparent 1:3 stoichiometry could be explained, for example, with the exit of an additional HCO_3^- ion via NBCe1-A. Alternatively, the apparent necessity to invoke a 1:3 stoichiometry could be the result of measurement resolution—that is, using available macroscopic measurements of $[\text{Na}^+]$ and $[\text{HCO}_3^-]$ near the inner and outer sides of the membrane rather than the relevant but unavailable measurements in the nanodomains adjacent to NBCe1-A.

Recent work is consistent with the notion that the receptor protein tyrosine phosphatase- γ (RPTP γ) at the BLM modulates H^+ secretion/ HCO_3^- reabsorption by activating a signaling mechanism in response to changes in basolateral $[\text{CO}_2]$ and $[\text{HCO}_3^-]$, [137–140].

6.1.1. Subcellular Localizations of CA Isozymes

CA II is present in the cytosol, and the glycosylphosphatidylinositol (GPI)-linked CA IV is expressed on both AM and BLM (less on the BLM) of the S1 and S2 segments of the PT [120,141]. CA XII is expressed only on the BLM [9].

Regarding RPTP γ , previous studies from our group suggest that the extracellular CA-like domain (CALD) senses CO_2 or HCO_3^- and the phosphatase domain turns on a downstream signaling cascade that reaches key acid–base transporters [137,138,140]. Interestingly, the CALD of RPTP γ , compared to CA II, lacks several key residues necessary for catalysis, including two of the three histidine residues essential for coordinating Zn^{2+} . If a physiological role of RPTP γ is indeed to sense basolateral CO_2 and HCO_3^- , one would expect it to lack catalytic activity (i.e., the molecule should not interconvert the solutes that it is detecting), as is indeed the case [142,143].

6.1.2. Functional Interactions with Acid–Base Transporters

As illustrated in Figure 5, the role of apical CA IV in HCO_3^- reabsorption is to convert luminal HCO_3^- to CO_2 for uptake across the AM. The role of cytosolic CA II is to convert the CO_2 entering across the AM to HCO_3^- and H^+ . Thus, both CA IV and CA II enhance the gradient that favors CO_2 uptake across the AM into the PT cell. CA II also provides cytosolic H^+ for extrusion by NHE3 and V-type H^+ pump across the AM, and HCO_3^- (which generates CO_3^{2-}) for transport by NBCe1-A across the BLM.

One group, following the lead of others working on AE1 in RBCs, reports that CA II binds to the C-terminus of NBCe1-A, creating a transport metabolon that enhances NBCe1-A activity [144,145]. In addition, others have reported that CA IV binds to the 4th extracellular loop of NBCe1-A, also stimulating NBCe1-A activity [146]. These papers are consistent with the idea that cytosolic CA II provides the substrate for NBCe1-A (HCO_3^- or CO_3^{2-}), while CA IV at the outer surface of the BLM dissipates the substrate [146]. However, our group detected neither binding of CA II to NBCe1-A, nor acceleration of transport, even after fusing CA II to the C-terminus of NBCe1-A [147–149]. Moreover, our recent work (pH₅ experiments of Figure 2 in ref. [73]) shows that CA IV activity— \pm expression or \pm ACZ—does not affect the NBCe1-A current (and therefore transport) induced by identical electrical driving forces [73]. As noted in our discussion of Figure 3, if HCO_3^- or CO_3^{2-} is the transported ion, little is gained by interconverting HCO_3^- and CO_2 . On the other hand, if CO_2 is the transported species, this interconversion has major effects on enhancing diffusion.

Here, in light of our findings that NBCe1-A transports CO_3^{2-} , we suggest that the role of CA IV at the BLM is to minimize local basolateral pH changes caused by CO_3^{2-} transport. Figure 6 shows the effects of HCO_3^- vs. CO_3^{2-} efflux on pH_{OS} in the presence (solid black trace) and absence (dashed red trace) of CA IV. If NBCe1-A were to transport HCO_3^- , then CA IV would accentuate the alkalinity of the extracellular surface. If NBCe1-A were to transport CO_3^{2-} , CA IV would reduce the alkalinity. In preliminary work, we increased peritubular $[\text{K}^+]$ to depolarize mouse PTs (thereby driving Na^+ and HCO_3^- into the PT cell) and observed the expected decrease in pH_{OS}. Performing this maneuver in the presence

of a peritubular CA inhibitor markedly increased the magnitude of the pH_{OS} decrease. These observations are consistent with the CO_3^{2-} transport model (Figure 6B). However, because PTs express many acid–base transporters, further investigations—for example, the use of PTs from knockout (KO) mice lacking specific acid–base transporters—are needed.

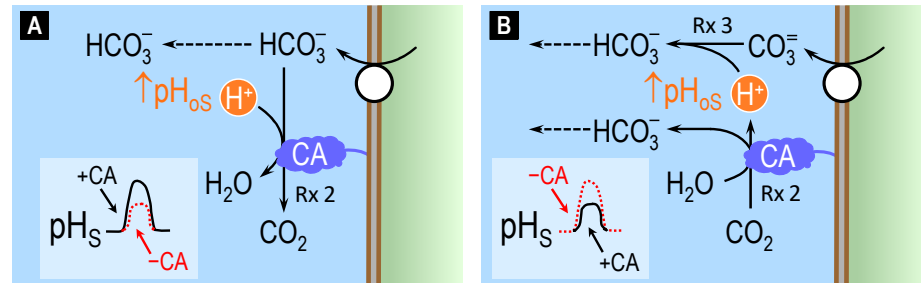


Figure 6. Theory of bicarbonate vs. carbonate efflux across cell membranes. (A) The exit of HCO_3^- leads to the consumption of H^+ (i.e., an increase in pH_{OS} ; inset, lower left corner: solid black trace) via the CA-catalyzed reaction $\text{HCO}_3^- + \text{H}^+ \rightarrow \text{CO}_2 + \text{H}_2\text{O}$ (indicated as ‘Rx 2’) at the outer surface (oS) of the cell membrane. Blocking CA (i.e., applying a CA inhibitor) reduces H^+ consumption (i.e., the rise in pH_{OS} ; dashed red trace). (B) The exit of CO_3^{2-} leads to the consumption of H^+ (i.e., an increase in pH_{OS} ; solid black trace) via the reaction $\text{CO}_3^{2-} + \text{H}^+ \rightarrow \text{HCO}_3^-$ (indicated as ‘Rx 3’) at the outer surface of the cell membrane. Blocking CA (i.e., applying a CA inhibitor) reduces production of H^+ (by ‘Rx 2’) for subsequent consumption via ‘Rx 3’. Thus, CA inhibition amplifies the rise in pH_{OS} (dashed red trace). Rx = reaction; the number following the abbreviation ‘Rx’ indicates the numbering of the reaction in the main text. CA = carbonic anhydrase.

Regarding a potential physiological role for CA XII at the BLM, we suggest that this enzyme, as CA IV, minimizes pH_{OS} changes at the BLM.

To summarize the actions of CAs in the PT, the apical CA IV and cytosolic CA II are complementary in accelerating the transmembrane CO_2 flux [56–58]. By converting CO_2 to the far-more-abundant HCO_3^- , CA II also accelerates the flux of “carbon” from the apical to the basolateral membrane. In the process, CA II also provides cytosolic substrates for apical H^+ extrusion and basolateral “ HCO_3^- ” efflux. The CA IV and XII at the BLM, however, do not play a substantial (or measurable) role in dissipating the “product” of NBCe1-A activity (i.e., the product being the appearance of CO_3^{2-} in the extracellular nanodomain near NBCe1-A). Instead, these CAs stabilize pH in this nanodomain.

6.2. Thick Ascending Limb

Approximately 10–15% of filtered HCO_3^- is reabsorbed in the TAL. The mechanism of HCO_3^- reabsorption in the TAL (Figure 7) is very similar to that in the S1 and S2 segments of the PT (Figure 5). In the TAL, NHE3/NHE2 and the V-type H^+ pump extrude H^+ across the AM [150]. In the lumen, the secreted H^+ combines with HCO_3^- , producing CO_2 and H_2O . Because the AM of the TAL is tight to NH_3 and water and, to date, no CO_2 -conducting membrane proteins (e.g., AQP) have been identified at the AM, the newly formed CO_2 enters the cell likely via diffusion only. Apical CA IV and cytosolic CA II, by maximizing the transmembrane CO_2 gradient across the AM, enhance CO_2 influx across the AM. Once inside the cytosol, the CO_2 combines with H_2O to form HCO_3^- and H^+ . In contrast to PTs, where NBCe1-A exports Na^+ and CO_3^{2-} across the BLM, here in the TAL, AE2 exchanges cytosolic HCO_3^- for Cl^- at the BLM. In addition to AE2, investigators have identified NBCn1 and (in rat) NBCn2 in the BLM of the TAL [131,151–153]. Because NBCn1 and NBCn2 normally operate in an inward direction [154], it seems unlikely that they contribute to HCO_3^- reabsorption per se. Instead, their roles may be to “facilitate” transcellular NH_4^+ transport from the TAL to the collecting duct [155,156].

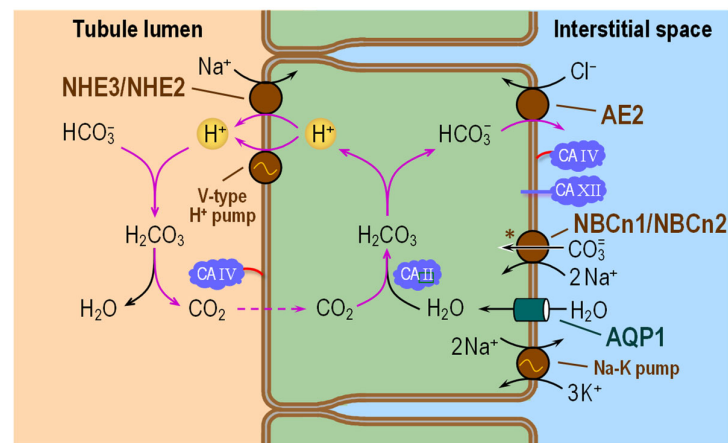


Figure 7. Cell model of HCO_3^- reabsorption in the thick ascending limb. In the lumen, filtered HCO_3^- and H^+ —secreted by NHE3/NHE2 and V-type H^+ pump—react to form CO_2 and H_2O under the catalytic action of CA IV. Apical entry of CO_2 and basolateral entry of H_2O via AQP1 lead to the intracellular formation of HCO_3^- and H^+ under the catalytic action of CA II. AE2 carries HCO_3^- out of the cell across the basolateral membrane. The brown symbol ‘*’ near NBCn1/NBCn2 denotes uncertainty about NBCn1/NBCn2 stoichiometry. For details, see text. NHE3/NHE2 = Na-H exchanger 3/Na-H exchanger 2; V-type H^+ pump = Vacuolar-type H^+ pump (or V-ATPase); CA II, CA IV and CA XII = carbonic anhydrase II, IV and XII; AE2 = anion exchanger 2; AQP1 = aquaporin 1; NBCn1/NBCn2 = electroneutral Na/ HCO_3^- cotransporter 1/electroneutral Na/ HCO_3^- cotransporter 2.

The TAL reabsorbs luminal NH_4^+ via the Na-K-Cl cotransporter 2 (NKCC2) and the renal outer medullary K^+ channel (ROMK) [157,158]. Once inside the cell, NH_4^+ dissociates into NH_3 and H^+ . It has been suggested that NBCn1 and NBCn2 neutralize this H^+ , thereby enhancing the formation of intracellular NH_3 and promoting NH_3 diffusion through the cell to the BLM. There, the NH_3 exits the TAL cell, possibly via AQP1 [159], diffuses through the interstitial fluid, and finally crosses the BLM of the α -intercalated cell via RhBG and RhCG [155,156,160]. Consistent with this hypothesis, in vivo and in vitro studies show that metabolic acidosis (MAc) increases NBCn1 expression [131,155,161].

Note that in Figure 7 we illustrate NBCn1 and NBCn2 as moving CO_3^{2-} (rather than HCO_3^-) into the cell, consistent with preliminary data from our group. However, because this transporter is electroneutral, in Figure 7 we tentatively illustrate the cotransport of 2 Na^+ ions. Additional work is needed to elucidate the stoichiometry of NBCn1 and NBCn2.

6.2.1. Subcellular Localizations of CA Isozymes

CA II is present in the cytosol of virtually all renal cells except for those in the tip of Henle’s loop and the thin ascending limb [120]. Within Henle’s loop, CA IV and CA XII are present only in the TAL, with similar localization as in the PT (i.e., CA IV is in both the AM and BLM and CA XII in the BLM).

6.2.2. Functional Interactions with Acid–Base Transporters

As illustrated in Figure 7, the role of apical CA IV in HCO_3^- reabsorption is to convert luminal HCO_3^- to CO_2 for uptake across the AM. The role of cytosolic CA II is to promote the consumption of incoming CO_2 , thereby accelerating CO_2 influx, and to provide cytosolic H^+ for extrusion by NHE3/NHE2 and the V-type H^+ pump across the AM, and HCO_3^- for export by AE2 across the BLM. These roles of apical CA IV and cytosolic CA II are similar to those discussed above for the PT.

Some investigators have reported that CA II and AEs can physically interact, thereby stimulating AEs activity [162–165]. According to other reports, CA IV binds to the 4th extracellular loop of AE1 (probably also AE2 and AE3), also stimulating AE1 activity [166]. However, other studies have shown no evidence of direct binding of CA II to the C-terminus of AE1 [147,167].

The work of Piermarini and colleagues [147] confirmed that liquid-phase AE1-C terminus (Ct) can bind to solid-phase CA II when—as in the earlier work—they fused the AE1-Ct to GST (which, significantly, forms dimers). Piermarini et al. replicated these results for GST-NBCe1-Ct and GST-NDCBE-Ct (collectively SLC4-Ct). However, when they reversed the orientation and applied liquid-phase CA II to solid-phase GST-SLC4-Ct, they observed no binding. Even when CA II was in the solid phase, SLC4-Ct failed to bind in the absence of GST. Thus, the interaction between the Ct of AE1 (and also of NBCe1 and NDCBE) does indeed occur but is not physiologically relevant because it requires that (i) the Ct be fused to GST and (ii) the GST fusion protein be liquid phase.

Moreover, our recent work (Figure 6 and Supplemental Table 3A in ref. [73]) shows that in oocytes expressing AE1 (\pm CA IV or \pm ACZ) and exposed to Cl^- -free $\text{CO}_2/\text{HCO}_3^-$ solution, the presence of CA IV does not affect the rates of pH_i recovery [73]. These experiments follow the trans-side rule of Musa-Aziz et al. [56–58]: it is legitimate to use pH measurements to assess the impact of a CA on the activity of an acid–base transporter only if the CA and the pH probe are on opposite sides of the membrane (e.g., CA IV on the outside, pH on the inside). The earlier authors added the CA II to the cytosol and measured pH on the same side. In their experiments, they saw that CA II markedly accelerated the AE1-dependent pH_i changes. This would have occurred regardless of the effect (if any) of CA II on the transport rate because CA II—interposed between AE1 and the pH_i probe—was responsible for translating the HCO_3^- flux into a pH_i signal.

Aside from the experimental data, as noted above in our discussion of Figure 3 as well as in the above corresponding section for PT, if HCO_3^- or CO_3^{2-} is the transported ion, the advantage of a CA-catalyzed interconversion of HCO_3^- and CO_2 for “ HCO_3^- ” transport would be small.

Here, in light of our findings that AE1 transports HCO_3^- and that NBCn1 and NBCn2 appear to carry CO_3^{2-} we propose that the role of CA IV at the BLM is not related to AE2 but to NBCn1 and NBCn2. Thus, we suggest that the CA IV (and possibly CA XII) minimizes pH_{OS} changes at the BLM caused by CO_3^{2-} entry by NBCn1 and NBCn2 (see insert, lower left corner of panel B of Figure 4: solid black trace). This pH_{OS} stabilization would presumably be beneficial to other nearby pH-sensitive proteins.

6.3. Tubules Distal to the Thick Ascending Limb

We have seen that most HCO_3^- reabsorption occurs in the PTs (~80–85%) and the TAL (~10–15%). The remaining ~5–10% of HCO_3^- reabsorption occurs in the distal nephron (i.e., from the macula densa, which marks the beginning of the distal convoluted tubule through the inner medullary collecting duct).

Like the tubule segments from the beginning of the PT to the end of the TAL (which expresses NKCC2), the earliest tubule segment after the macula densa, the distal convoluted tubule 1 (DCT1), has one cell type. This DCT1 cell (which expresses the Na/Cl cotransporter NCC) does not appear to participate in acid–base transport. The next segment, the DCT2, has two cell types, DCT2 cells (with NCC + epithelial Na^+ channel ENaC) and intercalated cells (ICs), the latter of which do participate in acid–base transport. The third segment, the connecting tubule (CNT), has both CNT cells (ENaC + AQP2) and ICs. The fourth segment, the initial collecting tubule (ICT), also has two cell types, the segment-specific principal cells (PCs; ENaC + AQP2) and ICs. The fifth segment, which begins after the first confluence of ICTs, is identical to the ICT but has a new name, the cortical collecting tubule (CCT) or duct; it has both segment-specific PCs as well as ICs. The sixth post-macula-densa segment is the outer medullary collecting duct (OMCD), which again has segment-specific PCs as well as ICs. Finally, the inner medullary collecting duct (IMCD) has ICs in its initial part, but thereafter IMCD cells (AQP2 + UT-A1) [168–174]. The proportion of PCs versus ICs varies along the segments of the distal nephron, among and within species, and with physiological conditions [170,172,175].

Among the cell type listed above, only the ICs perform substantial transepithelial acid–base transport, with perhaps some contribution from the IMCD cells. The ICs comprise

three subtypes: type-A or α -ICs (dominant in OMCD), type-B or β -ICs (dominant in CNT through CCT), and non-A/non-B [172,175,176].

The α -ICs secrete H^+ into the tubule lumen and thus are responsible for reabsorbing the remaining 5–10% of filtered HCO_3^- that enters the distal nephron (Figure 8). These cells perform this task by secreting H^+ into the lumen via the V-type H^+ pump and the H^+/K^+ pump, both on the AM [176–178]. CA IV at the AM converts filtered luminal HCO_3^- and secreted H^+ to CO_2 and H_2O . CO_2 presumably enters the cell via the Rh proteins RhBG and RhCG [160]. In the cytosol, CA II catalyzes the conversion of the incoming CO_2 and H_2O to HCO_3^- and H^+ . The newly formed HCO_3^- exits the BLM through the renal variant of AE1 [176–178]. Note that the roles of apical CA IV and cytosolic CA II in the α -IC are similar to those discussed above for the PT and TAL cells.

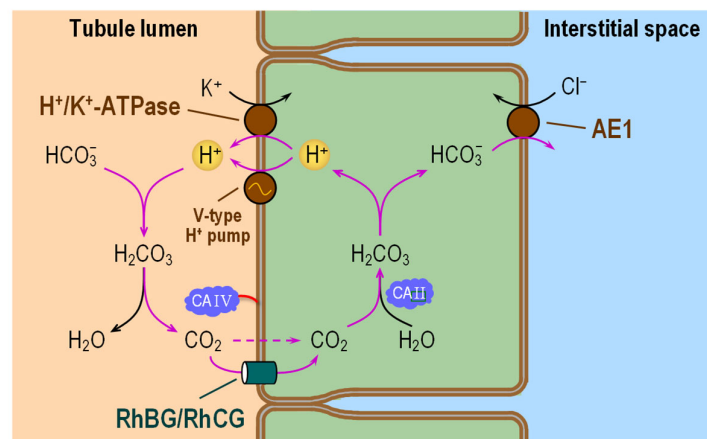


Figure 8. Cell model of HCO_3^- reabsorption in α -intercalated cells of the distal nephron. In the lumen, residual filtered HCO_3^- and H^+ —secreted by H^+/K^+ -pump and V-type H^+ pump—react to form CO_2 and H_2O under the catalytic action of CA IV. Apical entry of CO_2 via RhBG/RhCG leads to the intracellular formation of HCO_3^- and H^+ under the catalytic action of CA II. AE1 carries HCO_3^- out of the cell across the basolateral membrane. V-type H^+ pump = Vacuolar-type H^+ pump (or V-ATPase); RhBG/RhCG = Rh family B glycoprotein/Rh family C glycoprotein; CA II and CA IV = carbonic anhydrase II and IV; AE1 = anion exchanger 1.

The β -ICs cells secrete HCO_3^- into the tubule lumen [76,179]. Opposite to the α -ICs, the β -ICs express the V-type H^+ pump in the BLM, and a Cl^- - HCO_3^- exchanger in the AM. However, this apical Cl^- - HCO_3^- exchanger is pendrin (SLC26A4).

Non-A/non-B ICs, because they express both the V-type H^+ pump and pendrin in the AM [169,170], are intermediate between α -ICs and β -ICs (or, some say, a hybrid of the two), perhaps representing an intermediate state of cell differentiation [180]. For example, Purkerson and colleagues observed that MAc causes β -cells to become α -cells [181]. This transformation requires a large extracellular-matrix protein called hensin (from Japanese *henshin*, transformation) or deleted in malignant brain tumors 1 (DMBT1), as well as other proteins [180,182]. Indeed, mice without DMBT1 in the ICs have only a β -IC-like phenotype and develop MAc [183]. Inducing chronic MAc in rats leads to increased number of α -ICs. Similarly, inducing chronic metabolic alkalosis (MAlk) increases the number of β -ICs [180,184,185].

A recent study shows that the genetic deletion of NBCe1 (either global or PT-specific KO) eliminates the typical IC response to MAc (e.g., an increase in α -IC and decrease in β -ICs) and is consistent with the idea of a link between PTs and ICs [186].

6.3.1. Subcellular Localizations of CA Isozymes

High amount of CA II is present in the cytosol of all ICs in the distal nephron. CA IV is expressed only in the AM of α -ICs [120,126]. Principal cells also have CA II, but the amount is significantly lower than in the ICs [187].

6.3.2. Functional Interactions with Acid–Base Transporters

The sub-cellular localization of CAs, as well as the presence of a H⁺-secretory mechanism at the AM and a HCO₃[−]-exit mechanism at the BLM of α-ICs, provide all the tools necessary for these cells to perform H⁺ secretion in conjunction with HCO₃[−] reabsorption. Under normal physiological conditions, the contribution of ICs to whole-kidney HCO₃[−] reabsorption is relatively small. However, these cells may play a critical role as they “fine tune” urinary acid secretion. Moreover, it appears that these cells can compensate for impaired HCO₃[−] reabsorption in the preceding tubules [188]. A relatively low abundance of NCBTs (i.e., known or putative CO₃^{2−} transporters) on the BLM of ICs correlates with a relatively low expression of membrane-associated CAs at the BLM. This is consistent with our hypothesis that the role of membrane-associated CAs is not so much as to provide substrates to “HCO₃[−]” transporters as to stabilize pH in the nanodomains near H⁺ and CO₃^{2−} transporters. It will be informative to re-examine these issues with the accumulation of future data on the expression of NCBTs and CAs in the distal nephron.

7. Conclusions

CA activity has long been recognized as critically important for normal physiological function. For this reason, since the discovery of the first CA, investigators have focused considerable attention on the identification of CAs in a wide range of cells, how these CAs respond to physiological and pathophysiological challenges, and—using tools of molecular biophysics—the mechanisms of action of the CAs. Because of the fundamental role of CAs in acid–base homeostasis, some of these studies have focused on the interactions of CAs with acid–base transporters. As illustrated for the PT, TAL, and α-IC, the role of apical CA IV and cytosolic CA II is to accelerate CO₂ influx across the AM, to speed “carbon” diffusion from AM to BLM, and to provide H⁺ and HCO₃[−] as substrates for apical H⁺ extrusion and basolateral “HCO₃[−]” transport via members of the SLC4 family. Whereas the role of apical CA IV is to accelerate CO₂ influx across apical membranes (i.e., PT, TAL, and α-IC), the role of basolateral CA IV in the renal PT is to provide the H⁺ necessary to titrate the newly transported CO₃^{2−} to HCO₃[−]. By preventing an excessive rise in pH_{OS}, basolateral CA IV (and CA XII) protects pH-sensitive processes near NBCe1-A at the outer surface of the BLM. We suggest that it is likely that membrane-associated CAs play similar buffering roles when coupled with other members of the SLC4 that carry CO₃^{2−}. These membrane-associated CAs would similarly minimize pH_{OS} changes near the H⁺-extrusion mechanism but not near HCO₃[−] transporters (where they would accentuate pH_{OS} changes).

In the case of α- and β-ICs, the interconversion from one subtype to the other must involve substantial changes in the expression of CA IV, changes that coordinate with those in the acid–base transporters.

Author Contributions: Conceptualization, S.-K.L. and R.O.; writing—original draft preparation, S.-K.L. and R.O.; writing—review and editing, S.-K.L., W.F.B. and R.O.; funding acquisition, W.F.B. and R.O. All authors have read and agreed to the published version of the manuscript.

Funding: This work was supported by NIH grant R01-DK128315.

Institutional Review Board Statement: Not applicable.

Informed Consent Statement: Not applicable.

Data Availability Statement: Not applicable.

Acknowledgments: W.F.B. gratefully acknowledges the support of the Myers/Scarpa endowed chair.

Conflicts of Interest: The authors declare no conflict of interest.

References

1. Supuran, C.T. Carbonic Anhydrases and Metabolism. *Metabolites* **2018**, *8*, 25. [[CrossRef](#)] [[PubMed](#)]
2. Aspatwar, A.; Tolvanen, M.E.E.; Barker, H.; Syrjänen, L.; Valanne, S.; Purmonen, S.; Waheed, A.; Sly, W.S.; Parkkila, S. Carbonic Anhydrases in Metazoan Model Organisms: Molecules, Mechanisms, and Physiology. *Physiol. Rev.* **2022**, *102*, 1327–1383. [[CrossRef](#)] [[PubMed](#)]
3. Imtaiyaz Hassan, M.; Shajee, B.; Waheed, A.; Ahmad, F.; Sly, W.S. Structure, Function and Applications of Carbonic Anhydrase Isozymes. *Bioorg. Med. Chem.* **2013**, *21*, 1570–1582. [[CrossRef](#)] [[PubMed](#)]
4. Supuran, C.T. Structure and Function of Carbonic Anhydrases. *Biochem. J.* **2016**, *473*, 2023–2032. [[CrossRef](#)]
5. Occhipinti, R.; Boron, W.F. Role of Carbonic Anhydrases and Inhibitors in Acid-Base Physiology: Insights from Mathematical Modeling. *Int. J. Mol. Sci.* **2019**, *20*, 3841. [[CrossRef](#)]
6. Sly, W.S.; Hewett-Emmett, D.; Whyte, M.P.; Yu, Y.S.; Tashian, R.E. Carbonic Anhydrase II Deficiency Identified as the Primary Defect in the Autosomal Recessive Syndrome of Osteopetrosis with Renal Tubular Acidosis and Cerebral Calcification. *Proc. Natl. Acad. Sci. USA* **1983**, *80*, 2752–2756. [[CrossRef](#)]
7. Mori, S.; Kou, I.; Sato, H.; Emi, M.; Ito, H.; Hosoi, T.; Ikegawa, S. Nucleotide Variations in Genes Encoding Carbonic Anhydrase 8 and 10 Associated with Femoral Bone Mineral Density in Japanese Female with Osteoporosis. *J. Bone Miner. Metab.* **2009**, *27*, 213–216. [[CrossRef](#)]
8. Ivanov, S.V.; Kuzmin, I.; Wei, M.H.; Pack, S.; Geil, L.; Johnson, B.E.; Stanbridge, E.J.; Lerman, M.I. Down-Regulation of Transmembrane Carbonic Anhydrases in Renal Cell Carcinoma Cell Lines by Wild-Type von Hippel-Lindau Transgenes. *Proc. Natl. Acad. Sci. USA* **1998**, *95*, 12596–12601. [[CrossRef](#)]
9. Parkkila, S.; Parkkila, A.K.; Saarnio, J.; Kivelä, J.; Karttunen, T.J.; Kaunisto, K.; Waheed, A.; Sly, W.S.; Türeci, O.; Virtanen, I.; et al. Expression of the Membrane-Associated Carbonic Anhydrase Isozyme XII in the Human Kidney and Renal Tumors. *J. Histochem. Cytochem. Off. J. Histochem. Soc.* **2000**, *48*, 1601–1608. [[CrossRef](#)]
10. Pastorekova, S.; Parkkila, S.; Zavada, J. Tumor-Associated Carbonic Anhydrases and Their Clinical Significance. *Adv. Clin. Chem.* **2006**, *42*, 167–216.
11. Haapasalo, J.; Hilvo, M.; Nordfors, K.; Haapasalo, H.; Parkkila, S.; Hyrskyluoto, A.; Rantala, I.; Waheed, A.; Sly, W.S.; Pastorekova, S.; et al. Identification of an Alternatively Spliced Isoform of Carbonic Anhydrase XII in Diffusely Infiltrating Astrocytic Gliomas. *Neuro-Oncology* **2008**, *10*, 131–138. [[CrossRef](#)]
12. Watson, P.H.; Chia, S.K.; Wykoff, C.C.; Han, C.; Leek, R.D.; Sly, W.S.; Gatter, K.C.; Ratcliffe, P.; Harris, A.L. Carbonic Anhydrase XII Is a Marker of Good Prognosis in Invasive Breast Carcinoma. *Br. J. Cancer* **2003**, *88*, 1065–1070. [[CrossRef](#)]
13. Supuran, C.T. Emerging Role of Carbonic Anhydrase Inhibitors. *Clin. Sci. Lond. Engl.* **2021**, *135*, 1233–1249. [[CrossRef](#)]
14. Supuran, C.T. Carbonic Anhydrase Inhibitors. *Bioorg. Med. Chem. Lett.* **2010**, *20*, 3467–3474. [[CrossRef](#)]
15. Supuran, C.T.; Scozzafava, A.; Casini, A. Carbonic Anhydrase Inhibitors. *Med. Res. Rev.* **2003**, *23*, 146–189. [[CrossRef](#)]
16. Supuran, C.T. Carbonic Anhydrase Inhibitors as Emerging Agents for the Treatment and Imaging of Hypoxic Tumors. *Expert Opin. Investig. Drugs* **2018**, *27*, 963–970. [[CrossRef](#)]
17. Courcier, J.; de la Taille, A.; Nourieh, M.; Leguérney, I.; Lassau, N.; Ingels, A. Carbonic Anhydrase IX in Renal Cell Carcinoma, Implications for Disease Management. *Int. J. Mol. Sci.* **2020**, *21*, 7146. [[CrossRef](#)]
18. Ozensoy Guler, O.; Supuran, C.T.; Capasso, C. Carbonic Anhydrase IX as a Novel Candidate in Liquid Biopsy. *J. Enzyme Inhib. Med. Chem.* **2020**, *35*, 255–260. [[CrossRef](#)]
19. Haapasalo, J.; Nordfors, K.; Haapasalo, H.; Parkkila, S. The Expression of Carbonic Anhydrases II, IX and XII in Brain Tumors. *Cancers* **2020**, *12*, 1723. [[CrossRef](#)]
20. Meldrum, N.U.; Roughton, F.J. Carbonic Anhydrase. Its Preparation and Properties. *J. Physiol.* **1933**, *80*, 113–142. [[CrossRef](#)]
21. Rickli, E.E.; Ghazanfar, S.A.; Gibbons, B.H.; Edsall, J.T. Carbonic Anhydrases from Human Erythrocytes: Preparation and Properties of Two Enzymes. *J. Biol. Chem.* **1964**, *239*, 1065–1078. [[CrossRef](#)] [[PubMed](#)]
22. Nyman, P.O. Purification and Properties of Carbonic Anhydrase from Human Erythrocytes. *Biochim. Biophys. Acta* **1961**, *52*, 1–12. [[CrossRef](#)]
23. Lindskog, S. Purification and Properties of Bovine Erythrocyte Carbonic Anhydrase. *Biochim. Biophys. Acta* **1960**, *39*, 218–226. [[CrossRef](#)] [[PubMed](#)]
24. Dobyan, D.C.; Bulger, R.E. Renal Carbonic Anhydrase. *Am. J. Physiol.* **1982**, *243*, F311–F324. [[CrossRef](#)] [[PubMed](#)]
25. Jensen, E.L.; Clement, R.; Kosta, A.; Maberly, S.C.; Gontero, B. A New Widespread Subclass of Carbonic Anhydrase in Marine Phytoplankton. *ISME J.* **2019**, *13*, 2094–2106. [[CrossRef](#)]
26. Del Prete, S.; Nocentini, A.; Supuran, C.T.; Capasso, C. Bacterial ι -Carbonic Anhydrase: A New Active Class of Carbonic Anhydrase Identified in the Genome of the Gram-Negative Bacterium *Burkholderia Territorii*. *J. Enzyme Inhib. Med. Chem.* **2020**, *35*, 1060–1068. [[CrossRef](#)]
27. Nocentini, A.; Supuran, C.T.; Capasso, C. An Overview on the Recently Discovered Iota-Carbonic Anhydrases. *J. Enzyme Inhib. Med. Chem.* **2021**, *36*, 1988–1995. [[CrossRef](#)]
28. Mboge, M.Y.; Mahon, B.P.; McKenna, R.; Frost, S.C. Carbonic Anhydrases: Role in pH Control and Cancer. *Metabolites* **2018**, *8*, 19. [[CrossRef](#)]
29. Lomelino, C.L.; Andring, J.T.; McKenna, R. Crystallography and Its Impact on Carbonic Anhydrase Research. *Int. J. Med. Chem.* **2018**, *2018*, 9419521. [[CrossRef](#)]

30. Syrjänen, L.; Tolvanen, M.; Hilvo, M.; Olatubosun, A.; Innocenti, A.; Scozzafava, A.; Leppiniemi, J.; Niederhauser, B.; Hytönen, V.P.; Gorr, T.A.; et al. Characterization of the First Beta-Class Carbonic Anhydrase from an Arthropod (*Drosophila melanogaster*) and Phylogenetic Analysis of Beta-Class Carbonic Anhydrases in Invertebrates. *BMC Biochem.* **2010**, *11*, 28. [[CrossRef](#)]
31. Zolfaghari Emameh, R.; Barker, H.; Tolvanen, M.E.E.; Ortutay, C.; Parkkila, S. Bioinformatic Analysis of Beta Carbonic Anhydrase Sequences from Protozoans and Metazoans. *Parasit. Vectors* **2014**, *7*, 38. [[CrossRef](#)]
32. Supuran, C.T. Carbonic Anhydrases: Novel Therapeutic Applications for Inhibitors and Activators. *Nat. Rev. Drug Discov.* **2008**, *7*, 168–181. [[CrossRef](#)]
33. Del Prete, S.; Vullo, D.; Fisher, G.M.; Andrews, K.T.; Poulsen, S.-A.; Capasso, C.; Supuran, C.T. Discovery of a New Family of Carbonic Anhydrases in the Malaria Pathogen *Plasmodium falciparum*—The η -Carbonic Anhydrases. *Bioorg. Med. Chem. Lett.* **2014**, *24*, 4389–4396. [[CrossRef](#)]
34. Kikutani, S.; Nakajima, K.; Nagasato, C.; Tsuji, Y.; Miyatake, A.; Matsuda, Y. Thylakoid Luminal θ -Carbonic Anhydrase Critical for Growth and Photosynthesis in the Marine Diatom *Phaeodactylum tricornutum*. *Proc. Natl. Acad. Sci. USA* **2016**, *113*, 9828–9833. [[CrossRef](#)]
35. Ferry, J.G. The Gamma Class of Carbonic Anhydrases. *Biochim. Biophys. Acta* **2010**, *1804*, 374–381. [[CrossRef](#)]
36. Alber, B.E.; Colangelo, C.M.; Dong, J.; Stålhandske, C.M.; Baird, T.T.; Tu, C.; Fierke, C.A.; Silverman, D.N.; Scott, R.A.; Ferry, J.G. Kinetic and Spectroscopic Characterization of the Gamma-Carbonic Anhydrase from the Methanoarchaeon *Methanosarcina thermophila*. *Biochemistry* **1999**, *38*, 13119–13128. [[CrossRef](#)]
37. Amata, O.; Marino, T.; Russo, N.; Toscano, M. Catalytic Activity of a ζ -Class Zinc and Cadmium Containing Carbonic Anhydrase. Compared Work Mechanisms. *Phys. Chem. Chem. Phys. PCCP* **2011**, *13*, 3468–3477. [[CrossRef](#)]
38. Hirakawa, Y.; Senda, M.; Fukuda, K.; Yu, H.Y.; Ishida, M.; Taira, M.; Kinbara, K.; Senda, T. Characterization of a Novel Type of Carbonic Anhydrase That Acts without Metal Cofactors. *BMC Biol.* **2021**, *19*, 105. [[CrossRef](#)]
39. Jewell, D.A.; Tu, C.K.; Paranawithana, S.R.; Tanhauser, S.M.; LoGrasso, P.V.; Laipis, P.J.; Silverman, D.N. Enhancement of the Catalytic Properties of Human Carbonic Anhydrase III by Site-Directed Mutagenesis. *Biochemistry* **1991**, *30*, 1484–1490. [[CrossRef](#)]
40. Jackman, J.E.; Merz, K.M.; Fierke, C.A. Disruption of the Active Site Solvent Network in Carbonic Anhydrase II Decreases the Efficiency of Proton Transfer. *Biochemistry* **1996**, *35*, 16421–16428. [[CrossRef](#)]
41. Khalifah, R.G. The Carbon Dioxide Hydration Activity of Carbonic Anhydrase. I. Stop-Flow Kinetic Studies on the Native Human Isoenzymes B and C. *J. Biol. Chem.* **1971**, *246*, 2561–2573. [[CrossRef](#)] [[PubMed](#)]
42. Dodgson, S.J.; Shank, R.P.; Maryanoff, B.E. Topiramate as an Inhibitor of Carbonic Anhydrase Isoenzymes. *Epilepsia* **2000**, *41*, 35–39. [[CrossRef](#)]
43. Fujikawa-Adachi, K.; Nishimori, I.; Taguchi, T.; Onishi, S. Human Mitochondrial Carbonic Anhydrase VB: cDNA cloning, mRNA expression, subcellular localization, and mapping to chromosome X. *J. Biol. Chem.* **1999**, *274*, 21228–21233. [[CrossRef](#)] [[PubMed](#)]
44. Nagao, Y.; Batanian, J.R.; Clemente, M.F.; Sly, W.S. Genomic Organization of the Human Gene (CA5) and Pseudogene for Mitochondrial Carbonic Anhydrase V and Their Localization to Chromosomes 16q and 16p. *Genomics* **1995**, *28*, 477–484. [[CrossRef](#)] [[PubMed](#)]
45. Silverman, D.N.; Lindskog, S. The Catalytic Mechanism of Carbonic Anhydrase: Implications of a Rate-Limiting Protolysis of Water. *Acc. Chem. Res.* **1988**, *21*, 30–36. [[CrossRef](#)]
46. Liljas, A.; Carlsson, M.; Håkansson, K.; Lindahl, M.; Svensson, L.A.; Wehnert, A.; Cruickshank, D.W.J.; Helliwell, J.R.; Johnson, L.N.; Moffat, K.; et al. Laue and Monochromatic Crystallography on Carbonic Anhydrase. *Philos. Trans. R. Soc. Lond. Ser. Phys. Eng. Sci.* **1992**, *340*, 301–309. [[CrossRef](#)]
47. Bertini, I.; Luchinat, C.; Rosi, M.; Sgamellotti, A.; Tarantelli, F. pKa of Zinc-Bound Water and Nucleophilicity of Hydroxo-Containing Species. Ab Initio Calculations on Models for Zinc Enzymes. *Inorg. Chem.* **1990**, *29*, 1460–1463. [[CrossRef](#)]
48. Ataie, N.J.; Hoang, Q.Q.; Zahniser, M.P.D.; Tu, Y.; Milne, A.; Petsko, G.A.; Ringe, D. Zinc Coordination Geometry and Ligand Binding Affinity: The Structural and Kinetic Analysis of the Second-Shell Serine 228 Residue and the Methionine 180 Residue of the Aminopeptidase from *Vibrio proteolyticus*. *Biochemistry* **2008**, *47*, 7673–7683. [[CrossRef](#)]
49. Goto, M.; Takahashi, T.; Yamashita, F.; Koreeda, A.; Mori, H.; Ohta, M.; Arakawa, Y. Inhibition of the Metallo-Beta-Lactamase Produced from *Serratia marcescens* by Thiol Compounds. *Biol. Pharm. Bull.* **1997**, *20*, 1136–1140. [[CrossRef](#)]
50. Chegwidden, W.W.R.; Carter, N.N.D.; Edwards, Y.Y.H. *The Carbonic Anhydrases*; Springer: Berlin/Heidelberg, Germany, 2000; ISBN 3-7643-5670-7.
51. Tu, C.K.; Silverman, D.N.; Forsman, C.; Jonsson, B.H.; Lindskog, S. Role of Histidine 64 in the Catalytic Mechanism of Human Carbonic Anhydrase II Studied with a Site-Specific Mutant. *Biochemistry* **1989**, *28*, 7913–7918. [[CrossRef](#)]
52. Engstrand, C.; Forsman, C.; Liang, Z.; Lindskog, S. Proton Transfer Roles of Lysine 64 and Glutamic Acid 64 Replacing Histidine 64 in the Active Site of Human Carbonic Anhydrase II. *Biochim. Biophys. Acta* **1992**, *1122*, 321–326. [[CrossRef](#)]
53. Krebs, J.F.; Ippolito, J.A.; Christianson, D.W.; Fierke, C.A. Structural and Functional Importance of a Conserved Hydrogen Bond Network in Human Carbonic Anhydrase II. *J. Biol. Chem.* **1993**, *268*, 27458–27466. [[CrossRef](#)]
54. Liang, Z.; Xue, Y.; Behravan, G.; Jonsson, B.H.; Lindskog, S. Importance of the Conserved Active-Site Residues Tyr7, Glu106 and Thr199 for the Catalytic Function of Human Carbonic Anhydrase II. *Eur. J. Biochem.* **1993**, *211*, 821–827. [[CrossRef](#)]
55. Aspatwar, A.; Tolvanen, M.E.; Parkkila, S. Phylogeny and Expression of Carbonic Anhydrase-Related Proteins. *BMC Mol. Biol.* **2010**, *11*, 25. [[CrossRef](#)]

56. Musa-Aziz, R.; Occhipinti, R.; Boron, W.F. Evidence from Simultaneous Intracellular- and Surface-pH Transients That Carbonic Anhydrase II Enhances CO₂ Fluxes across *Xenopus* Oocytes Plasma Membranes. *Am. J. Physiol. Cell Physiol.* **2014**, *307*, C791–C813. [[CrossRef](#)]
57. Musa-Aziz, R.; Occhipinti, R.; Boron, W.F. Evidence from Simultaneous Intracellular- and Surface-pH Transients That Carbonic Anhydrase IV Enhances CO₂ Fluxes across *Xenopus* Oocyte Plasma Membranes. *Am. J. Physiol. Cell Physiol.* **2014**, *307*, C814–C840. [[CrossRef](#)]
58. Occhipinti, R.; Musa-Aziz, R.; Boron, W.F. Evidence from Mathematical Modeling That Carbonic Anhydrase II and IV Enhance CO₂ Fluxes across *Xenopus* Oocytes Plasma Membranes. *Am. J. Physiol. Cell Physiol.* **2014**, *307*, C841–C858. [[CrossRef](#)]
59. Gutknecht, J.; Bisson, M.A.; Tosteson, F.C. Diffusion of Carbon Dioxide through Lipid Bilayer Membranes: Effects of Carbonic Anhydrase, Bicarbonate, and Unstirred Layers. *J. Gen. Physiol.* **1977**, *69*, 779–794. [[CrossRef](#)]
60. Boron, W.F. Intracellular pH-Regulating Mechanism of the Squid Axon. Relation between the External Na⁺ and HCO₃⁻ Dependences. *J. Gen. Physiol.* **1985**, *85*, 325–345. [[CrossRef](#)]
61. Jentsch, T.J.; Schwartz, P.; Schill, B.S.; Langner, B.; Lepple, A.P.; Keller, S.K.; Wiederholt, M. Kinetic Properties of the Sodium Bicarbonate (Carbonate) Symport in Monkey Kidney Epithelial Cells (BSC-1). Interactions between Na⁺, HCO₃⁻, and pH. *J. Biol. Chem.* **1986**, *261*, 10673–10679. [[CrossRef](#)]
62. Boron, W.F.; Knakal, R.C. Intracellular pH-Regulating Mechanism of the Squid Axon. Interaction between DNDS and Extracellular Na⁺ and HCO₃⁻. *J. Gen. Physiol.* **1989**, *93*, 123–150. [[CrossRef](#)] [[PubMed](#)]
63. Boron, W.F.; Knakal, R.C. Na⁺-Dependent Cl⁻-HCO₃⁻ Exchange in the Squid Axon. Dependence on Extracellular pH. *J. Gen. Physiol.* **1992**, *99*, 817–837. [[CrossRef](#)] [[PubMed](#)]
64. Boron, W.F.; Russell, J.M. Stoichiometry and Ion Dependencies of the Intracellular-pH-Regulating Mechanism in Squid Giant Axons. *J. Gen. Physiol.* **1983**, *81*, 373–399. [[CrossRef](#)] [[PubMed](#)]
65. Soleimani, M.; Aronson, P.S. Ionic Mechanism of Na⁺-HCO₃⁻ Cotransport in Rabbit Renal Basolateral Membrane Vesicles. *J. Biol. Chem.* **1989**, *264*, 18302–18308. [[CrossRef](#)]
66. Zhu, Q.; Shao, X.M.; Kao, L.; Azimov, R.; Weinstein, A.M.; Newman, D.; Liu, W.; Kurtz, I. Missense Mutation T485S Alters NBCe1-A Electrogenicity Causing Proximal Renal Tubular Acidosis. *Am. J. Physiol. Cell Physiol.* **2013**, *305*, C392–C405. [[CrossRef](#)]
67. Lee, S.-K.; Boron, W.F.; Parker, M.D. Substrate Specificity of the Electrogenic Sodium/Bicarbonate Cotransporter NBCe1-A (SLC4A4, Variant A) from Humans and Rabbits. *Am. J. Physiol. Renal Physiol.* **2013**, *304*, F883–F899. [[CrossRef](#)]
68. Seki, G.; Coppola, S.; Yoshitomi, K.; Burckhardt, B.C.; Samarzija, I.; Müller-Berger, S.; Frömter, E. On the Mechanism of Bicarbonate Exit from Renal Proximal Tubular Cells. *Kidney Int.* **1996**, *49*, 1671–1677. [[CrossRef](#)]
69. Boron, W.F. Evaluating the Role of Carbonic Anhydrases in the Transport of HCO₃⁻-Related Species. *Biochim. Biophys. Acta* **2010**, *1804*, 410–421. [[CrossRef](#)]
70. Grichtchenko, I.I.; Chesler, M. Depolarization-Induced Acid Secretion in Gliotic Hippocampal Slices. *Neuroscience* **1994**, *62*, 1057–1070. [[CrossRef](#)]
71. Occhipinti, R.; Lu, J.; Boron, W.F. Is the Electrogenic Na/HCO₃ Cotransporter a CO₂ Channel? *FASEB J.* **2016**, *30*, 971.2. [[CrossRef](#)]
72. Moss, F.J.; Occhipinti, R.; Zeise, B.; Zhao, P.; Wang, D.-K.; Lu, J.; Boron, W.F. The Electrogenic Sodium Bicarbonate Cotransporter NBCe1 as a Conduit for CO₂. *FASEB J.* **2019**, *33*, 544.3. [[CrossRef](#)]
73. Lee, S.-K.; Occhipinti, R.; Moss, F.J.; Parker, M.D.; Grichtchenko, I.I.; Boron, W.F. Distinguishing among HCO₃⁻, CO₃⁼, and H⁺ as Substrates of Proteins That Appear to Be “Bicarbonate” Transporters. *J. Am. Soc. Nephrol.* **2023**, *34*, 40–54. [[CrossRef](#)]
74. Alper, S.L.; Sharma, A.K. The SLC26 Gene Family of Anion Transporters and Channels. *Mol. Asp. Med.* **2013**, *34*, 494–515. [[CrossRef](#)]
75. Amlal, H.; Petrovic, S.; Xu, J.; Wang, Z.; Sun, X.; Barone, S.; Soleimani, M. Deletion of the Anion Exchanger Slc26a4 (Pendrin) Decreases Apical Cl(-)/HCO₃(-) Exchanger Activity and Impairs Bicarbonate Secretion in Kidney Collecting Duct. *Am. J. Physiol. Cell Physiol.* **2010**, *299*, C33–C41. [[CrossRef](#)]
76. Royaux, I.E.; Wall, S.M.; Karniski, L.P.; Everett, L.A.; Suzuki, K.; Knepper, M.A.; Green, E.D. Pendrin, Encoded by the Pendred Syndrome Gene, Resides in the Apical Region of Renal Intercalated Cells and Mediates Bicarbonate Secretion. *Proc. Natl. Acad. Sci. USA* **2001**, *98*, 4221–4226. [[CrossRef](#)]
77. Cordat, E.; Casey, J.R. Bicarbonate Transport in Cell Physiology and Disease. *Biochem. J.* **2009**, *417*, 423. [[CrossRef](#)]
78. Tsuganezawa, H.; Kobayashi, K.; Iyori, M.; Araki, T.; Koizumi, A.; Watanabe, S.; Kaneko, A.; Fukao, T.; Monkawa, T.; Yoshida, T.; et al. A New Member of the HCO₃⁻ Transporter Superfamily Is an Apical Anion Exchanger of Beta-Intercalated Cells in the Kidney. *J. Biol. Chem.* **2001**, *276*, 8180–8189. [[CrossRef](#)]
79. Ko, S.B.H.; Luo, X.; Hager, H.; Rojek, A.; Choi, J.Y.; Licht, C.; Suzuki, M.; Muallem, S.; Nielsen, S.; Ishibashi, K. AE4 Is a DIDS-Sensitive Cl⁻/HCO₃⁻ Exchanger in the Basolateral Membrane of the Renal CCD and the SMG Duct. *Am. J. Physiol. Cell Physiol.* **2002**, *283*, C1206–C1218. [[CrossRef](#)]
80. Xu, J.; Barone, S.; Petrovic, S.; Wang, Z.; Seidler, U.; Riederer, B.; Ramaswamy, K.; Dudeja, P.K.; Shull, G.E.; Soleimani, M. Identification of an Apical Cl⁻/HCO₃⁻ Exchanger in Gastric Surface Mucous and Duodenal Villus Cells. *Am. J. Physiol. Gastrointest. Liver Physiol.* **2003**, *285*, G1225–G1234. [[CrossRef](#)]
81. Chambrey, R.; Kurth, I.; Peti-Peterdi, J.; Houillier, P.; Purkerson, J.M.; Leviel, F.; Hentschke, M.; Zdebik, A.A.; Schwartz, G.J.; Hübner, C.A.; et al. Renal Intercalated Cells Are Rather Energized by a Proton than a Sodium Pump. *Proc. Natl. Acad. Sci. USA* **2013**, *110*, 7928–7933. [[CrossRef](#)]

82. Peña-Münzenmayer, G.; Catalán, M.A.; Kondo, Y.; Jaramillo, Y.; Liu, F.; Shull, G.E.; Melvin, J.E. Ae4 (Slc4a9) Anion Exchanger Drives Cl⁻ Uptake-Dependent Fluid Secretion by Mouse Submandibular Gland Acinar Cells. *J. Biol. Chem.* **2015**, *290*, 10677–10688. [[CrossRef](#)]
83. Myers, E.J.; Marshall, A.; Jennings, M.L.; Parker, M.D. Mouse Slc4a11 Expressed in *Xenopus* Oocytes Is an Ideally Selective H⁺/OH⁻ Conductance Pathway That Is Stimulated by Rises in Intracellular and Extracellular pH. *Am. J. Physiol.-Cell Physiol.* **2016**, *311*, C945–C959. [[CrossRef](#)] [[PubMed](#)]
84. Kao, L.; Azimov, R.; Abuladze, N.; Newman, D.; Kurtz, I. Human SLC4A11-C Functions as a DIDS-Stimulatable H⁺(OH⁻) Permeation Pathway: Partial Correction of R109H Mutant Transport. *Am. J. Physiol. Cell Physiol.* **2015**, *308*, C176–C188. [[CrossRef](#)] [[PubMed](#)]
85. Bruce, L.J.; Tanner, M.J. Erythroid Band 3 Variants and Disease. *Baillieres Best Pract. Res. Clin. Haematol.* **1999**, *12*, 637–654. [[CrossRef](#)] [[PubMed](#)]
86. Alloisio, N.; Texier, P.; Vallier, A.; Ribeiro, M.L.; Morlé, L.; Bozon, M.; Bursaux, E.; Maillet, P.; Gonçalves, P.; Tanner, M.J.; et al. Modulation of Clinical Expression and Band 3 Deficiency in Hereditary Spherocytosis. *Blood* **1997**, *90*, 414–420. [[CrossRef](#)]
87. Ribeiro, M.L.; Alloisio, N.; Almeida, H.; Gomes, C.; Texier, P.; Lemos, C.; Mimoso, G.; Morlé, L.; Bey-Cabet, F.; Rudigoz, R.C.; et al. Severe Hereditary Spherocytosis and Distal Renal Tubular Acidosis Associated with the Total Absence of Band 3. *Blood* **2000**, *96*, 1602–1604.
88. Igarashi, T.; Inatomi, J.; Sekine, T.; Cha, S.H.; Kanai, Y.; Kunimi, M.; Tsukamoto, K.; Satoh, H.; Shimadzu, M.; Tozawa, F.; et al. Mutations in SLC4A4 Cause Permanent Isolated Proximal Renal Tubular Acidosis with Ocular Abnormalities. *Nat. Genet.* **1999**, *23*, 264–266. [[CrossRef](#)]
89. Demirci, F.Y.K.; Chang, M.-H.; Mah, T.S.; Romero, M.F.; Gorin, M.B. Proximal Renal Tubular Acidosis and Ocular Pathology: A Novel Missense Mutation in the Gene (SLC4A4) for Sodium Bicarbonate Cotransporter Protein (NBCe1). *Mol. Vis.* **2006**, *12*, 324–330.
90. Suzuki, M.; Van Paesschen, W.; Stalmans, I.; Horita, S.; Yamada, H.; Bergmans, B.A.; Legius, E.; Riant, F.; De Jonghe, P.; Li, Y.; et al. Defective Membrane Expression of the Na⁺-HCO₃⁻ Cotransporter NBCe1 Is Associated with Familial Migraine. *Proc. Natl. Acad. Sci. USA* **2010**, *107*, 15963–15968. [[CrossRef](#)]
91. Alka, K.; Casey, J.R. Bicarbonate Transport in Health and Disease. *IUBMB Life* **2014**, *66*, 596–615. [[CrossRef](#)]
92. Romero, M.F.; Chen, A.-P.; Parker, M.D.; Boron, W.F. The SLC4 Family of Bicarbonate (HCO₃⁻) Transporters. *Mol. Asp. Med.* **2013**, *34*, 159–182. [[CrossRef](#)]
93. Parker, M.D.; Boron, W.F. The Divergence, Actions, Roles, and Relatives of Sodium-Coupled Bicarbonate Transporters. *Physiol. Rev.* **2013**, *93*, 803–959. [[CrossRef](#)]
94. Pushkin, A.; Kurtz, I. SLC4 Base (HCO₃⁻, CO₃²⁻) Transporters: Classification, Function, Structure, Genetic Diseases, and Knockout Models. *Am. J. Physiol. Renal Physiol.* **2006**, *290*, F580–F599. [[CrossRef](#)]
95. Lee, S.-K.; Boron, W.F.; Parker, M.D. Monitoring Ion Activities in and around Cells Using Ion-Selective Liquid-Membrane Microelectrodes. *Sensors* **2013**, *13*, 984–1003. [[CrossRef](#)]
96. Fagerberg, L.; Hallström, B.M.; Oksvold, P.; Kampf, C.; Djureinovic, D.; Odeberg, J.; Habuka, M.; Tahmasebpour, S.; Danielsson, A.; Edlund, K.; et al. Analysis of the Human Tissue-Specific Expression by Genome-Wide Integration of Transcriptomics and Antibody-Based Proteomics. *Mol. Cell. Proteomics MCP* **2014**, *13*, 397–406. [[CrossRef](#)]
97. Hilvo, M.; Tolvanen, M.; Clark, A.; Shen, B.; Shah, G.N.; Waheed, A.; Halmi, P.; Hänninen, M.; Hämäläinen, J.M.; Vihinen, M.; et al. Characterization of CA XV, a New GPI-Anchored Form of Carbonic Anhydrase. *Biochem. J.* **2005**, *392*, 83–92. [[CrossRef](#)]
98. Davenport, H.W.; Wilhelm, A.E. Renal Carbonic Anhydrase. *Proc. Soc. Exp. Biol. Med.* **1941**, *48*, 53–56. [[CrossRef](#)]
99. Hober, R. Effect of Some Sulfonamides on Renal Secretion. *Proc. Soc. Exp. Biol. Med.* **1942**, *49*, 87–90. [[CrossRef](#)]
100. Pitts, R.F.; Alexander, R.S. The Renal Reabsorptive Mechanism for Inorganic Phosphate in Normal and Acidotic Dogs. *Am. J. Physiol.* **1944**, *142*, 648–662. [[CrossRef](#)]
101. Pitts, R.F.; Alexander, R.S. The Nature of the Renal Tubular Mechanism for Acidifying the Urine. *Am. J. Physiol.-Leg. Content* **1945**, *144*, 239–254. [[CrossRef](#)]
102. Pitts, R.F. The Renal Regulation of Acid Base Balance with Special Reference to the Mechanism for Acidifying the Urine. *Science* **1945**, *102*, 49–54. [[CrossRef](#)] [[PubMed](#)]
103. Davenport, H.W. Carbonic Anhydrase in Tissues Other than Blood. *Physiol. Rev.* **1946**, *26*, 560–573. [[CrossRef](#)] [[PubMed](#)]
104. Berliner, R.W.; Orloff, J. Carbonic Anhydrase Inhibitors. *Pharmacol. Rev.* **1956**, *8*, 137–174. [[PubMed](#)]
105. Smith, H.W. *The Physiology of the Kidney*; Oxford University Press: Oxford, UK, 1937.
106. Gottschalk, C.W.; Berliner, R.W.; Giebisch, G.H. *Renal Physiology: People and Ideas*; Springer: Berlin/Heidelberg, Germany, 2013; ISBN 978-1-4614-7545-3.
107. Nicholson, T.F. The Site of Acidification of the Urine in the Dog's Kidney. *Can. J. Biochem. Physiol.* **1957**, *35*, 419–423. [[CrossRef](#)] [[PubMed](#)]
108. Walker, A.M.; Bott, P.A.; Oliver, J.; MacDowell, M.C. The Collection and Analysis of Fluid from Single Nephrons of the Mammalian Kidney. *Am. J. Physiol.-Leg. Content* **1941**, *134*, 580–595. [[CrossRef](#)]
109. Berliner, R.W. Some aspects of ion exchange in electrolyte transport by the renal tubules. In *Metabolic Aspects of Transport Across Cell Membranes*; University of Wisconsin Press: Madison, WI, USA, 1957; pp. 203–220.

110. Gottschalk, C.W.; Lassiter, W.E.; Mylle, M. Localization of Urine Acidification in the Mammalian Kidney. *Am. J. Physiol.-Leg. Content* **1960**, *198*, 581–585. [[CrossRef](#)]
111. DuBose, T.D., Jr. Carbonic Anhydrase-Dependent Bicarbonate Transport in the Kidney. *Ann. N. Y. Acad. Sci.* **1984**, *429*, 528–537. [[CrossRef](#)]
112. Lucci, M.S.; Tinker, J.P.; Weiner, I.M.; DuBose, T.D. Function of Proximal Tubule Carbonic Anhydrase Defined by Selective Inhibition. *Am. J. Physiol.-Ren. Physiol.* **1983**, *245*, F443–F449. [[CrossRef](#)]
113. Lucci, M.S.; Pucacco, L.R.; DuBose, T.D.; Kokko, J.P.; Carter, N.W. Direct Evaluation of Acidification by Rat Proximal Tubule: Role of Carbonic Anhydrase. *Am. J. Physiol.* **1980**, *238*, F372–F379. [[CrossRef](#)]
114. Rector, F.C.; Carter, N.W.; Seldin, D.W. The Mechanism of Bicarbonate Reabsorption in the Proximal and Distal Tubules of the Kidney. *J. Clin. Investig.* **1965**, *44*, 278–290. [[CrossRef](#)]
115. DuBose, T.D.; Pucacco, L.R.; Carter, N.W. Determination of Disequilibrium pH in the Rat Kidney in Vivo: Evidence of Hydrogen Secretion. *Am. J. Physiol.* **1981**, *240*, F138–F146. [[CrossRef](#)]
116. McKinney, T.D.; Burg, M.B. Bicarbonate Transport by Rabbit Cortical Collecting Tubules. Effect of Acid and Alkali Loads in Vivo on Transport in Vitro. *J. Clin. Investig.* **1977**, *60*, 766–768. [[CrossRef](#)]
117. Burg, M.; Green, N. Bicarbonate Transport by Isolated Perfused Rabbit Proximal Convolved Tubules. *Am. J. Physiol.* **1977**, *233*, F307–F314. [[CrossRef](#)]
118. McKinney, T.D.; Burg, M.B. Bicarbonate and Fluid Absorption by Renal Proximal Straight Tubules. *Kidney Int.* **1977**, *12*, 1–8. [[CrossRef](#)]
119. Good, D.W.; Knepper, M.A.; Burg, M.B. Ammonia and Bicarbonate Transport by Thick Ascending Limb of Rat Kidney. *Am. J. Physiol.-Ren. Physiol.* **1984**, *247*, F35–F44. [[CrossRef](#)]
120. Purkerson, J.M.; Schwartz, G.J. The Role of Carbonic Anhydrases in Renal Physiology. *Kidney Int.* **2007**, *71*, 103–115. [[CrossRef](#)]
121. Lönnerholm, G.; Wistrand, P.J. Carbonic Anhydrase in the Human Kidney: A Histochemical and Immunocytochemical Study. *Kidney Int.* **1984**, *25*, 886–898. [[CrossRef](#)]
122. Wistrand, J.; Lindahl, S.; Wählstrand, T. Human Renal Carbonic Anhydrase. Purification and Properties. *Eur. J. Biochem. FEBS* **1975**, *57*, 189–195. [[CrossRef](#)]
123. Lönnerholm, G.; Wistrand, P.J. Membrane-Bound Carbonic Anhydrase CA IV in the Human Kidney. *Acta Physiol. Scand.* **1991**, *141*, 231–234. [[CrossRef](#)]
124. Wistrand, P.J. Human Renal Cytoplasmic Carbonic Anhydrase. Tissue Levels and Kinetic Properties under near Physiological Conditions. *Acta Physiol. Scand.* **1980**, *109*, 239–248. [[CrossRef](#)]
125. Maren, T.H.; Ellison, A.C. A Study of Renal Carbonic Anhydrase. *Mol. Pharmacol.* **1967**, *3*, 503–508. [[PubMed](#)]
126. Schwartz, G.J.; Kittelberger, A.M.; Barnhart, D.A.; Vijayakumar, S. Carbonic Anhydrase IV Is Expressed in H(+)-Secreting Cells of Rabbit Kidney. *Am. J. Physiol. Ren. Physiol.* **2000**, *278*, F894–F904. [[CrossRef](#)] [[PubMed](#)]
127. Wistrand, P.J.; Kinne, R. Carbonic Anhydrase Activity of Isolated Brush Border and Basal-Lateral Membranes of Renal Tubular Cells. *Pflugers Arch.* **1977**, *370*, 121–126. [[CrossRef](#)] [[PubMed](#)]
128. Murer, H.; Hopfer, U.; Kinne, R. Sodium/Proton Antiport in Brush-Border-Membrane Vesicles Isolated from Rat Small Intestine and Kidney. *Biochem. J.* **1976**, *154*, 597–604. [[CrossRef](#)]
129. Kinsella, J.L.; Aronson, P.S. Properties of the Na⁺-H⁺ Exchanger in Renal Microvillus Membrane Vesicles. *Am. J. Physiol.* **1980**, *238*, F461–F469. [[CrossRef](#)]
130. Boron, W.F.; Boulpaep, E.L. Intracellular pH Regulation in the Renal Proximal Tubule of the Salamander. Na⁺-H⁺ Exchange. *J. Gen. Physiol.* **1983**, *81*, 29–52. [[CrossRef](#)]
131. Guo, Y.-M.; Liu, Y.; Liu, M.; Wang, J.-L.; Xie, Z.-D.; Chen, K.-J.; Wang, D.-K.; Occhipinti, R.; Boron, W.F.; Chen, L.-M. Na⁺/HCO₃⁻ Cotransporter NBCn2 Mediates HCO₃⁻ Reclamation in the Apical Membrane of Renal Proximal Tubules. *J. Am. Soc. Nephrol. JASN* **2017**, *28*, 2409–2419. [[CrossRef](#)]
132. Nakhoul, N.L.; Davis, B.A.; Romero, M.F.; Boron, W.F. Effect of Expressing the Water Channel Aquaporin-1 on the CO₂ Permeability of *Xenopus* Oocytes. *Am. J. Physiol.* **1998**, *274*, C543–C548. [[CrossRef](#)]
133. Zhou, Y.; Bouyer, P.; Boron, W.F. Evidence That AQP1 Is a Functional CO₂ Channel in Proximal Tubules. *FASEB J.* **2006**, *20*, A1225–A1226. [[CrossRef](#)]
134. Cooper, G.J.; Boron, W.F. Effect of PCMBs on CO₂ Permeability of *Xenopus* Oocytes Expressing Aquaporin 1 or Its C189S Mutant. *Am. J. Physiol.* **1998**, *275*, C1481–C1486. [[CrossRef](#)]
135. Preston, G.M.; Carroll, T.P.; Guggino, W.B.; Agre, P. Appearance of Water Channels in *Xenopus* Oocytes Expressing Red Cell CHIP28 Protein. *Science* **1992**, *256*, 385–387. [[CrossRef](#)]
136. Boron, W.F.; Boulpaep, E.L. Intracellular pH Regulation in the Renal Proximal Tubule of the Salamander. Basolateral HCO₃⁻ Transport. *J. Gen. Physiol.* **1983**, *81*, 53–94. [[CrossRef](#)]
137. Zhou, Y.; Skelton, L.A.; Xu, L.; Chandler, M.P.; Berthiaume, J.M.; Boron, W.F. Role of Receptor Protein Tyrosine Phosphatase γ in Sensing Extracellular CO₂ and HCO₃⁻. *J. Am. Soc. Nephrol. JASN* **2016**, *27*, 2616–2621. [[CrossRef](#)]
138. Skelton, L.A.; Boron, W.F. Effect of Acute Acid-Base Disturbances on ErbB1/2 Tyrosine Phosphorylation in Rabbit Renal Proximal Tubules. *Am. J. Physiol. Ren. Physiol.* **2013**, *305*, F1747–F1764. [[CrossRef](#)]
139. Skelton, L.A.; Boron, W.F.; Zhou, Y. Acid-Base Transport by the Renal Proximal Tubule. *J. Nephrol.* **2010**, *23* (Suppl. S16), S4–S18.

140. Skelton, L.A.; Boron, W.F. Effect of Acute Acid-Base Disturbances on the Phosphorylation of Phospholipase C- β 1 and Erk1/2 in the Renal Proximal Tubule. *Physiol. Rep.* **2015**, *3*, e12280. [[CrossRef](#)]
141. Brown, D.; Zhu, X.L.; Sly, W.S. Localization of Membrane-Associated Carbonic Anhydrase Type IV in Kidney Epithelial Cells. *Proc. Natl. Acad. Sci. USA* **1990**, *87*, 7457–7461. [[CrossRef](#)]
142. Barnea, G.; Silvennoinen, O.; Shaanan, B.; Honegger, A.M.; Canoll, P.D.; D'Eustachio, P.; Morse, B.; Levy, J.B.; Laforgia, S.; Huebner, K. Identification of a Carbonic Anhydrase-like Domain in the Extracellular Region of RPTP Gamma Defines a New Subfamily of Receptor Tyrosine Phosphatases. *Mol. Cell. Biol.* **1993**, *13*, 1497–1506.
143. Skelton, L.; Musa-Aziz, R.; Qin, X.; Boron, W.F. Mutations That “Restore” Enzymatic Activity to the Carbonic Anhydrase-like Domain (CALD) of Receptor Protein Tyrosine Phosphatase Gamma (RPTP γ): Importance of Shuttle Hits and CO₂ Binding Site. *J. Am. Soc. Nephrol.* **2010**, *21*, 252A.
144. Gross, E.; Pushkin, A.; Abuladze, N.; Fedotoff, O.; Kurtz, I. Regulation of the Sodium Bicarbonate Cotransporter KNBC1 Function: Role of Asp⁹⁸⁶, Asp⁹⁸⁸ and KNBC1-Carbonic Anhydrase II Binding. *J. Physiol.* **2002**, *544*, 679–685. [[CrossRef](#)]
145. Pushkin, A.; Abuladze, N.; Gross, E.; Newman, D.; Tatishchev, S.; Lee, I.; Fedotoff, O.; Bondar, G.; Azimov, R.; Ngyuen, M.; et al. Molecular Mechanism of KNBC1-Carbonic Anhydrase II Interaction in Proximal Tubule Cells. *J. Physiol.* **2004**, *559*, 55–65. [[CrossRef](#)]
146. Alvarez, B.V.; Loisselle, F.B.; Supuran, C.T.; Schwartz, G.J.; Casey, J.R. Direct Extracellular Interaction between Carbonic Anhydrase IV and the Human NBC1 Sodium/Bicarbonate Co-Transporter. *Biochemistry* **2003**, *42*, 12321–12329. [[CrossRef](#)] [[PubMed](#)]
147. Piermarini, P.M.; Kim, E.Y.; Boron, W.F. Evidence against a Direct Interaction between Intracellular Carbonic Anhydrase II and Pure C-Terminal Domains of SLC4 Bicarbonate Transporters. *J. Biol. Chem.* **2007**, *282*, 1409–1421. [[CrossRef](#)] [[PubMed](#)]
148. Lu, J.; Daly, C.M.; Parker, M.D.; Gill, H.S.; Piermarini, P.M.; Pelletier, M.F.; Boron, W.F. Effect of Human Carbonic Anhydrase II on the Activity of the Human Electrogenic Na/HCO₃ Cotransporter NBCe1-A in *Xenopus* Oocytes. *J. Biol. Chem.* **2006**, *281*, 19241–19250. [[CrossRef](#)] [[PubMed](#)]
149. Moss, F.J.; Boron, W.F. Carbonic Anhydrases Enhance Activity of Endogenous Na-H Exchangers and Not the Electrogenic Na/HCO₃ Cotransporter NBCe1-A, Expressed in *Xenopus* Oocytes. *J. Physiol.* **2020**, *598*, 5821–5856. [[CrossRef](#)]
150. Zacchia, M.; Capolongo, G.; Rinaldi, L.; Capasso, G. The Importance of the Thick Ascending Limb of Henle’s Loop in Renal Physiology and Pathophysiology. *Int. J. Nephrol. Renov. Dis.* **2018**, *11*, 81–92. [[CrossRef](#)]
151. Vorum, H.; Kwon, T.H.; Fulton, C.; Simonsen, B.; Choi, I.; Boron, W.; Maunsbach, A.B.; Nielsen, S.; Aalkjaer, C. Immunolocalization of Electroneutral Na-HCO₃[−] Cotransporter in Rat Kidney. *Am. J. Physiol. Ren. Physiol.* **2000**, *279*, F901–F909. [[CrossRef](#)]
152. Boedtker, E.; Praetorius, J.; Fuchtbauer, E.-M.; Aalkjaer, C. Antibody-Independent Localization of the Electroneutral Na⁺-HCO₃[−] Cotransporter NBCn1 (Slc4a7) in Mice. *Am. J. Physiol. Cell Physiol.* **2008**, *294*, C591–C603. [[CrossRef](#)]
153. Wang, J.-L.; Wang, X.-Y.; Wang, D.-K.; Parker, M.D.; Musa-Aziz, R.; Popple, J.; Guo, Y.-M.; Min, T.-X.; Xia, T.; Tan, M.; et al. Multiple Acid-Base and Electrolyte Disturbances Upregulate NBCn1, NBCn2, IRBIT and L-IRBIT in the MTAL. *J. Physiol.* **2020**, *598*, 3395–3415. [[CrossRef](#)]
154. Choi, I.; Aalkjaer, C.; Boulpaep, E.L.; Boron, W.F. An Electroneutral Sodium/Bicarbonate Cotransporter NBCn1 and Associated Sodium Channel. *Nature* **2000**, *405*, 571–575. [[CrossRef](#)]
155. Odgaard, E.; Jakobsen, J.K.; Frische, S.; Praetorius, J.; Nielsen, S.; Aalkjaer, C.; Leipziger, J. Basolateral Na⁺-Dependent HCO₃[−] Transporter NBCn1-Mediated HCO₃[−] Influx in Rat Medullary Thick Ascending Limb. *J. Physiol.* **2004**, *555*, 205–218. [[CrossRef](#)]
156. Lee, S.; Lee, H.J.; Yang, H.S.; Thornell, I.M.; Bevenssee, M.O.; Choi, I. Sodium-Bicarbonate Cotransporter NBCn1 in the Kidney Medullary Thick Ascending Limb Cell Line Is Upregulated under Acidic Conditions and Enhances Ammonium Transport. *Exp. Physiol.* **2010**, *95*, 926–937. [[CrossRef](#)]
157. Attmane-Elakeb, A.; Mount, D.B.; Sibella, V.; Vernimmen, C.; Hebert, S.C.; Bichara, M. Stimulation by in Vivo and in Vitro Metabolic Acidosis of Expression of RBSC-1, the Na⁺-K⁺(NH₄⁺)-2Cl[−] Cotransporter of the Rat Medullary Thick Ascending Limb. *J. Biol. Chem.* **1998**, *273*, 33681–33691. [[CrossRef](#)]
158. Jans, F.; Balut, C.; Ameloot, M.; Wouters, P.; Steels, P. Investigation of the Ba²⁺- Sensitive NH₄⁺ Transport Pathways in the Apical Cell Membrane of Primary Cultured Rabbit MTAL Cells. *Nephron Physiol.* **2007**, *106*, p45–p53. [[CrossRef](#)]
159. Cabral, P.D.; Herrera, M. Membrane-Associated Aquaporin-1 Facilitates Osmotically Driven Water Flux across the Basolateral Membrane of the Thick Ascending Limb. *Am. J. Physiol. Ren. Physiol.* **2012**, *303*, F621–F629. [[CrossRef](#)]
160. Geyer, R.R.; Parker, M.D.; Toye, A.M.; Boron, W.F.; Musa-Aziz, R. Relative CO₂/NH₃ Permeabilities of Human RhAG, RhBG and RhCG. *J. Membr. Biol.* **2013**, *246*, 915–926. [[CrossRef](#)]
161. Kwon, T.-H.; Fulton, C.; Wang, W.; Kurtz, I.; Frøkiær, J.; Aalkjaer, C.; Nielsen, S. Chronic Metabolic Acidosis Upregulates Rat Kidney Na-HCO₃[−] Cotransporters NBCn1 and NBC3 but Not NBC1. *Am. J. Physiol. Ren. Physiol.* **2002**, *282*, F341–F351. [[CrossRef](#)]
162. Sterling, D.; Reithmeier, R.A.; Casey, J.R. A Transport Metabolon. Functional Interaction of Carbonic Anhydrase II and Chloride/Bicarbonate Exchangers. *J. Biol. Chem.* **2001**, *276*, 47886–47894. [[CrossRef](#)]
163. Vince, J.W.; Reithmeier, R.A. Identification of the Carbonic Anhydrase II Binding Site in the Cl[−]/HCO₃[−] Anion Exchanger AE1. *Biochemistry* **2000**, *39*, 5527–5533. [[CrossRef](#)]
164. Vince, J.W.; Reithmeier, R.A. Carbonic Anhydrase II Binds to the Carboxyl Terminus of Human Band 3, the Erythrocyte Cl[−]/HCO₃[−] Exchanger. *J. Biol. Chem.* **1998**, *273*, 28430–28437. [[CrossRef](#)]

165. Vince, J.W.; Carlsson, U.; Reithmeier, R.A. Localization of the $\text{Cl}^-/\text{HCO}_3^-$ Anion Exchanger Binding Site to the Amino-Terminal Region of Carbonic Anhydrase II. *Biochemistry* **2000**, *39*, 13344–13349. [[CrossRef](#)] [[PubMed](#)]
166. Sterling, D.; Alvarez, B.V.; Casey, J.R. The Extracellular Component of a Transport Metabolon. Extracellular Loop 4 of the Human AE1 $\text{Cl}^-/\text{HCO}_3^-$ Exchanger Binds Carbonic Anhydrase IV. *J. Biol. Chem.* **2002**, *277*, 25239–25246. [[CrossRef](#)] [[PubMed](#)]
167. Al-Samir, S.; Papadopoulos, S.; Scheibe, R.J.; Meißner, J.D.; Cartron, J.-P.; Sly, W.S.; Alper, S.L.; Gros, G.; Endeward, V. Activity and Distribution of Intracellular Carbonic Anhydrase II and Their Effects on the Transport Activity of Anion Exchanger AE1/SLC4A1. *J. Physiol.* **2013**, *591*, 4963–4982. [[CrossRef](#)] [[PubMed](#)]
168. Kriz, W.; Kaissling, B. Chapter 20—Structural Organization of the Mammalian Kidney. In *Seldin and Giebisch's the Kidney*, 5th ed.; Alpern, R.J., Moe, O.W., Caplan, M., Eds.; Academic Press: Cambridge, MA, USA, 2013; pp. 595–691. ISBN 978-0-12-381462-3.
169. Teng-umnuay, P.; Verlander, J.W.; Yuan, W.; Tisher, C.C.; Madsen, K.M. Identification of Distinct Subpopulations of Intercalated Cells in the Mouse Collecting Duct. *J. Am. Soc. Nephrol. JASN* **1996**, *7*, 260–274. [[CrossRef](#)]
170. Kim, J.; Kim, Y.H.; Cha, J.H.; Tisher, C.C.; Madsen, K.M. Intercalated Cell Subtypes in Connecting Tubule and Cortical Collecting Duct of Rat and Mouse. *J. Am. Soc. Nephrol. JASN* **1999**, *10*, 1–12. [[CrossRef](#)]
171. Wall, S.M.; Verlander, J.W.; Romero, C.A. The Renal Physiology of Pendrin-Positive Intercalated Cells. *Physiol. Rev.* **2020**, *100*, 1119–1147. [[CrossRef](#)]
172. Chen, L.; Clark, J.Z.; Nelson, J.W.; Kaissling, B.; Ellison, D.H.; Knepper, M.A. Renal-Tubule Epithelial Cell Nomenclature for Single-Cell RNA-Sequencing Studies. *J. Am. Soc. Nephrol. JASN* **2019**, *30*, 1358–1364. [[CrossRef](#)]
173. Loffing, J.; Pietri, L.; Aregger, F.; Bloch-Faure, M.; Ziegler, U.; Meneton, P.; Rossier, B.C.; Kaissling, B. Differential Subcellular Localization of ENaC Subunits in Mouse Kidney in Response to High- and Low-Na Diets. *Am. J. Physiol. Ren. Physiol.* **2000**, *279*, F252–F258. [[CrossRef](#)]
174. Masilamani, S.; Kim, G.H.; Mitchell, C.; Wade, J.B.; Knepper, M.A. Aldosterone-Mediated Regulation of ENaC Alpha, Beta, and Gamma Subunit Proteins in Rat Kidney. *J. Clin. Investig.* **1999**, *104*, R19–R23. [[CrossRef](#)]
175. Roy, A.; Al-bataineh, M.M.; Pastor-Soler, N.M. Collecting Duct Intercalated Cell Function and Regulation. *Clin. J. Am. Soc. Nephrol. CJASN* **2015**, *10*, 305–324. [[CrossRef](#)]
176. Alper, S.L.; Natale, J.; Gluck, S.; Lodish, H.F.; Brown, D. Subtypes of Intercalated Cells in Rat Kidney Collecting Duct Defined by Antibodies against Erythroid Band 3 and Renal Vacuolar H^+ -ATPase. *Proc. Natl. Acad. Sci. USA* **1989**, *86*, 5429–5433. [[CrossRef](#)]
177. Brown, D.; Gluck, S.; Hartwig, J. Structure of the Novel Membrane-Coating Material in Proton-Secreting Epithelial Cells and Identification as an H^+ ATPase. *J. Cell Biol.* **1987**, *105*, 1637–1648. [[CrossRef](#)]
178. Brown, D.; Weyer, P.; Orci, L. Nonclathrin-Coated Vesicles Are Involved in Endocytosis in Kidney Collecting Duct Intercalated Cells. *Anat. Rec.* **1987**, *218*, 237–242. [[CrossRef](#)]
179. Brown, D.; Hirsch, S.; Gluck, S. An H^+ -ATPase in Opposite Plasma Membrane Domains in Kidney Epithelial Cell Subpopulations. *Nature* **1988**, *331*, 622–624. [[CrossRef](#)]
180. Al-Awqati, Q. Terminal Differentiation in Epithelia: The Role of Integrins in Hensin Polymerization. *Annu. Rev. Physiol.* **2011**, *73*, 401–412. [[CrossRef](#)]
181. Purkerson, J.M.; Tsuruoka, S.; Suter, D.Z.; Nakamori, A.; Schwartz, G.J. Adaptation to Metabolic Acidosis and Its Recovery Are Associated with Changes in Anion Exchanger Distribution and Expression in the Cortical Collecting Duct. *Kidney Int.* **2010**, *78*, 993–1005. [[CrossRef](#)]
182. Takito, J.; Hikita, C.; Al-Awqati, Q. Hensin, a New Collecting Duct Protein Involved in the in Vitro Plasticity of Intercalated Cell Polarity. *J. Clin. Investig.* **1996**, *98*, 2324–2331. [[CrossRef](#)]
183. Gao, X.; Eladari, D.; Leviel, F.; Tew, B.Y.; Miró-Julà, C.; Cheema, F.H.; Miller, L.; Nelson, R.; Paunescu, T.G.; McKee, M.; et al. Deletion of Hensin/DMBT1 Blocks Conversion of Beta- to Alpha-Intercalated Cells and Induces Distal Renal Tubular Acidosis. *Proc. Natl. Acad. Sci. USA* **2010**, *107*, 21872–21877. [[CrossRef](#)]
184. Bastani, B.; Purcell, H.; Hemken, P.; Trigg, D.; Gluck, S. Expression and Distribution of Renal Vacuolar Proton-Translocating Adenosine Triphosphatase in Response to Chronic Acid and Alkali Loads in the Rat. *J. Clin. Investig.* **1991**, *88*, 126–136. [[CrossRef](#)]
185. Sabolić, I.; Brown, D.; Gluck, S.L.; Alper, S.L. Regulation of AE1 Anion Exchanger and H^+ -ATPase in Rat Cortex by Acute Metabolic Acidosis and Alkalosis. *Kidney Int.* **1997**, *51*, 125–137. [[CrossRef](#)]
186. Verlander, J.W.; Lee, H.-W.; Wall, S.M.; Harris, A.N.; Weiner, I.D. The Proximal Tubule through an NBCe1-Dependent Mechanism Regulates Collecting Duct Phenotypic and Remodeling Responses to Acidosis. *Am. J. Physiol. Ren. Physiol.* **2023**, *324*, F12–F29. [[CrossRef](#)] [[PubMed](#)]
187. Kim, J.; Tisher, C.C.; Linser, P.J.; Madsen, K.M. Ultrastructural Localization of Carbonic Anhydrase II in Subpopulations of Intercalated Cells of the Rat Kidney. *J. Am. Soc. Nephrol. JASN* **1990**, *1*, 245–256. [[CrossRef](#)] [[PubMed](#)]
188. Nagami, G.T.; Hamm, L.L. Regulation of Acid-Base Balance in Chronic Kidney Disease. *Adv. Chronic Kidney Dis.* **2017**, *24*, 274–279. [[CrossRef](#)] [[PubMed](#)]

Disclaimer/Publisher's Note: The statements, opinions and data contained in all publications are solely those of the individual author(s) and contributor(s) and not of MDPI and/or the editor(s). MDPI and/or the editor(s) disclaim responsibility for any injury to people or property resulting from any ideas, methods, instructions or products referred to in the content.